

1 **Macroalgal influence on particulate organic matter sources and early transformation in an**  
2 **Arctic fjord**

3 Ashok S Jagtap<sup>1</sup>, Archana Singh<sup>1</sup>, Anand Jain<sup>1</sup>, Nandini Raj<sup>2</sup>, Manish Tiwari<sup>1</sup>

4 <sup>1</sup>National Centre for Polar and Ocean Research, Ministry of Earth Sciences, Vasco-da-Gama,  
5 Goa 403804, India

6 <sup>2</sup>Amity Institute of Biotechnology, Amity University, Uttar Pradesh 201313, India

7  
8 Correspondence to:

9 Ashok S. Jagtap ([ashokjagtap200@gmail.com](mailto:ashokjagtap200@gmail.com)),

10 Archana Singh ([archanasingh@ncpor.res.in](mailto:archanasingh@ncpor.res.in))

11  
12  
13 **Highlights**

- 14 • Macroalgal-dominated sites were observed with higher labile surface particulate organic  
15 carbon and nitrogen signatures compared to adjacent waters.
- 16 • Biochemical and biomolecular composition indicated lateral transport from macroalgal-  
17 beds with conservative reorganization.
- 18 • Brandal was identified as a model site for future biogeochemical studies related to  
19 macroalgal expansion in Kongsfjorden.

24 **Abstract**

25 Accelerated Arctic warming is promoting the expansion of coastal macroalgal habitats; yet their  
26 influence on pelagic organic carbon cycling remains unresolved. This study *investigates* the  
27 influence of macroalgal beds on the biochemical composition of surface particulate organic matter  
28 (POM) in Kongsfjorden, Svalbard, during late summer 2023. Surface waters were sampled at four  
29 macroalgal-dominated sites (MDS) and from adjacent waters (Adj-W) located 500 m and 1500 m  
30 away. A multi-proxy approach integrating elemental composition, stable isotopes, biopolymeric  
31 fractions, monosaccharides, and amino acids was used to trace macroalgal contributions and their  
32 lateral redistribution. Concentrations of particulate organic carbon, nitrogen, carbohydrates, and  
33 proteins were consistently higher at MDS than in Adj-W, indicating localized enrichment of  
34 biochemically labile organic matter within macroalgal habitats. *Molecular analyses further*  
35 *revealed elevated concentrations of macroalgal-associated sugars (glucose, galactose, fucose,*  
36 *mannuronic acid) and labile amino acids (Asp, Glu, Gly, Ser, Ala) reinforcing macroalgal-derived*  
37 *contributions to surface POM. While,  $\delta^{13}\text{C}_{\text{POC}}$  showed minimal spatial variation ( $-26.8$  to  $-29.1\%$ ),*  
38 *the biochemical and molecular signatures indicated a decreasing macroalgal contribution towards*  
39 *Adj-W, along with internal reorganization, suggesting lateral transport of macroalgal-derived*  
40 *POM with selective early-stage transformation.* Overall, these findings indicate that Arctic  
41 macroalgal beds act as dynamic coastal biogeochemical hotspots, redistributing and transforming  
42 organic carbon beyond their habitat.

43 **Keywords:** Arctic fjords; macroalgal-derived organic matter; coastal carbon cycling; lateral  
44 transport

45

46

47

48 **1. Introduction**

49 Accelerated warming of the Arctic has led to pronounced environmental changes, including a  
50 reduction in sea ice extent and thickness, intensified glacier melt, widespread permafrost thawing,  
51 and a shift toward more liquid precipitation (Dai et al., 2019; Rantanen et al., 2022). These changes  
52 are altering marine primary production (Attard et al., 2024), coastal carbon sources (Mathew et al.,  
53 2025), and nutrient dynamics within Arctic fjord systems (McGovern et al., 2020). Amid these  
54 environmental transformations, macroalgae have demonstrated ecological resilience and  
55 adaptability, enabling their expansion along Arctic coastlines (Assis et al., 2022). Recent estimates  
56 from species distribution modeling indicate a substantial increase in subtidal (45%) and intertidal  
57 (8%) brown macroalgal cover along the Arctic coastline over the past few decades (Krause-Jensen  
58 et al., 2020). This rapid and ongoing macroalgal expansion contributes substantially to coastal  
59 primary productivity and carbon dynamics in the Arctic (Attard et al., 2024; Krause-Jensen et al.,  
60 2020). Macroalgal biomass and condition are strongly shaped by local environmental variability,  
61 with runoff and site-specific forcing influencing kelp biochemistry and ecosystem functioning in  
62 Arctic coastal systems (Castro de la Guardia et al., 2025; Niedzwiedz et al., 2025). Comparable  
63 environment-driven changes in kelp biomass and distribution have been reported across the Arctic,  
64 including Greenland and the Canadian Arctic, indicating pan-Arctic rather than site-specific  
65 responses (Carlson et al., 2026; Filbee-Dexter and Wernberg, 2020; Krause-Jensen and Duarte,  
66 2016). Kelp forest structure shifted markedly, with a reduced depth distribution, a declining  
67 abundance of several kelp species, and an increasing dominance of *Alaria esculenta*, driven  
68 primarily by rising turbidity and coastal darkening rather than temperature alone, thereby  
69 reshaping kelp biomass, demography, and ecosystem functioning in Kongsfjorden (Düsedau et al.,

70 2024). Field experiments have also shown that macroalgal blades can lose approximately 3% of  
71 their total area per day due to mechanical stress, physical abrasion against rocky substrates,  
72 seasonal increases in tissue brittleness, and biological weakening by epiphytes. Which, provide a  
73 substantial and continuous input of macroalgal-derived material to the coastal particulate organic  
74 matter (POM) pool (Buchholz and Wiencke, 2016).

75         Macroalgal beds contribute a significant amount of macroalgal-derived organic carbon,  
76 approximately 60% as particulate organic carbon (POC), and approximately 30% as dissolved  
77 organic carbon (DOC) (Kennedy and Blain, 2025; Pessarrodona et al., 2022) to the surrounding  
78 environment, and play a crucial role in supporting secondary production via detrital food web and  
79 coastal Arctic carbon cycling (Pedersen et al., 2021; Renaud et al., 2015; Simpkins et al., 2025).  
80 Macroalgal POM appears in multiple forms, including whole thalli and tissue fragments, and is  
81 often buoyant due to structural features such as pneumatocysts, allowing particles to stay  
82 suspended in surface waters (Carlson et al., 2026; Kennedy and Blain, 2025). This buoyancy  
83 promotes extensive lateral transport across coastal and fjord systems, effectively linking benthic  
84 macroalgal production with pelagic environments and shaping the spatial distribution of organic  
85 carbon (Carlson et al., 2026; van der Mheen et al., 2024). A substantial fraction of the carbon  
86 produced in macroalgal beds is exported to surrounding environments, with only about 2%  
87 remaining and settling at the site of production (Kennedy and Blain, 2025; Krause-Jensen and  
88 Duarte, 2016; Pessarrodona et al., 2022). Macroalgal POM undergoes microbial-mediated  
89 transformation and degradation during transit and thereby affects biogeochemical processes in  
90 macroalgal beds as well as adjacent waters (Adj-W) (Duarte et al., 2013; Krause-Jensen and  
91 Duarte, 2016; Ortega et al., 2019). Biochemical compositional and lipid biomarker studies have  
92 shown hints of macroalgal contribution to POM (Singh et al., 2024b) and sediments (Roy et al.,

93 2025) in Kongsfjorden. Similarly, studies from saline lake system demonstrate that microbial  
94 transformations of organic matter require high-resolution molecular proxies to distinguish carbon  
95 sources (Jiang et al., 2022; Yang et al., 2020). However, the spatial variability and magnitude of  
96 macroalgal-derived organic carbon contributions to POM along coastal gradients remain poorly  
97 understood.

98 To resolve the sources and transformation pathways better, and to understand how the  
99 expansion of macroalgal forests will influence Arctic coastal biogeochemistry, a systematic  
100 biochemical characterization of POM in and around macroalgal-dominated sites is necessary.  
101 Thus, the present study investigated the biochemical composition of POM from the surface waters  
102 of Kongsfjorden (Svalbard) at four macroalgal-dominated sites (MDS), and their respective  
103 adjacent waters (Adj-W) located 500 m and 1500 m from the MDS sites. Here, we addressed two  
104 key questions: *(i) To what extent do the biochemical characteristics of surface POM at MDS reflect*  
105 *inputs from macroalgal-derived organic matter? (ii) How does the biochemical composition of*  
106 *POM change from MDS to Adj-W, and (iii) What do these changes reveal about the lateral*  
107 *transport and early alteration of macroalgal-derived organic matter?*

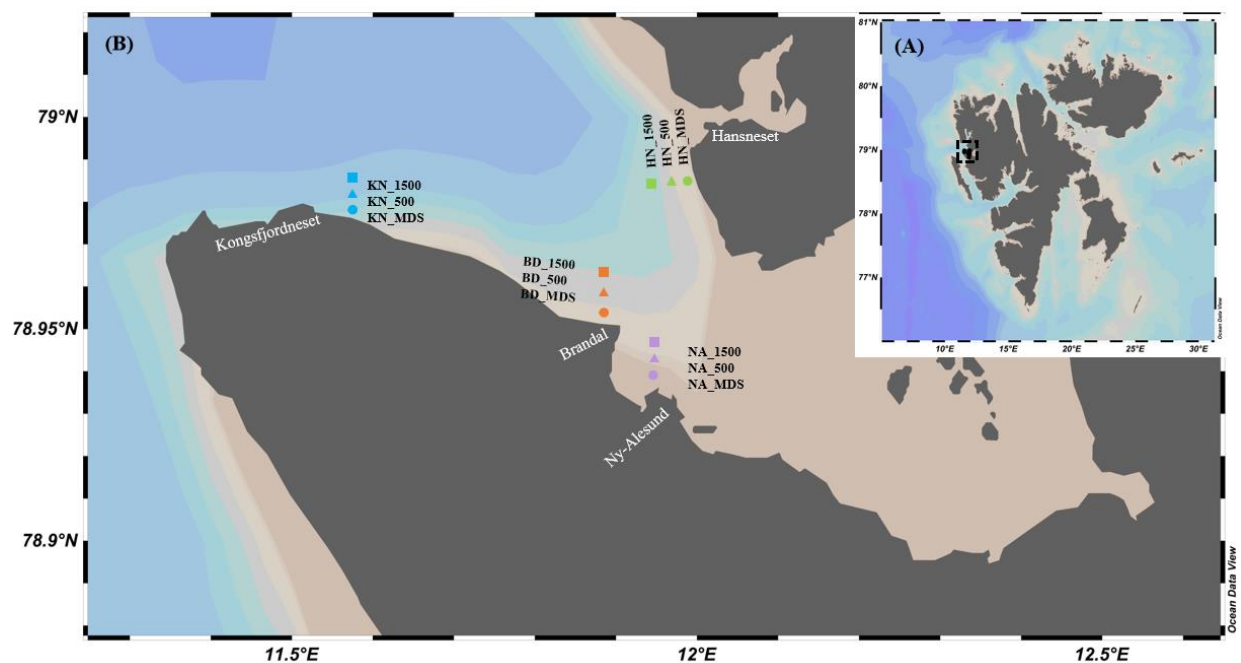
108

## 109 **Material and Methods**

### 110 **2.1 Sampling site and locations**

111 Surface water samples were collected during late summer 2023 (September–October) from four  
112 MDS distributed along and across the Kongsfjorden coast using the workboat Teisten, with a  
113 Niskin sampler deployed at 3 m depth, as well as from adjacent locations (Adj-W) located 500 m  
114 and 1500 m away from each MDS site (Figs. 1A and 1B). The seawater was pre-filtered using a

115 200  $\mu\text{m}$  mesh to remove larger particles. Seawater samples (3 L) were filtered using pre-combusted  
116 (4 hours at 450  $^{\circ}\text{C}$ ) 0.7  $\mu\text{m}$  pore size glass fiber filters (GF/F) to collect particulate matter.  
117 Immediately after filtration, the GF/F filters were stored at -80  $^{\circ}\text{C}$  until analysis. An aliquot of 100  
118 mL seawater sample for dissolved nutrients analysis was collected in high-density polyethylene  
119 bottles from each sampling location and stored at -80  $^{\circ}\text{C}$  until analysis.



120  
121 **Figure 1.** Study area and sampling locations in Svalbard (A) and the detailed map of sampling  
122 stations in Kongsfjorden (B) across nearshore macroalgal beds (MDS), mid-fjord (500 m), and  
123 offshore (1500 m) sites at BD, NA, KN, and HN.

124  
125 **2.2 Physicochemical characteristics of seawater**

126 The vertical profiles of temperature, salinity, and turbidity at each sampling location were recorded  
127 using an SBE 911 plus instrument (Seabird Electronics Inc., USA). The concentrations of  
128 dissolved nutrients (nitrate, nitrite, silicate, and phosphate) were determined using a Seal AA3

129 analytical autoanalyzer with a standard deviation of  $\pm 1\%$  and an  $R^2$  value of  $>0.99$  (Grasshoff et  
130 al., 2009). Chlorophyll *a* was extracted following (Singh et al., 2024a) with minor modifications.  
131 Briefly, GF/F filters were extracted in 90% acetone under low-light conditions by keeping them  
132 overnight at  $-20\text{ }^\circ\text{C}$ . The pigment extracts were centrifuged ( $10,000\times g$ ,  $4\text{ }^\circ\text{C}$ , 10 min), filtered ( $0.2$   
133  $\mu\text{m}$  PVDF), and analyzed using an Agilent 1200 HPLC with a ZORBAX 300 Extend-C8 column  
134 ( $1.1\text{ mL min}^{-1}$ ,  $40\text{ }^\circ\text{C}$ ). Pigments were separated using a reverse-phase methanol–ammonium  
135 acetate gradient and identified by comparing retention times and absorption spectra ( $250\text{--}850\text{ nm}$ )  
136 against a DHI chlorophyll-*a* standard.

137

### 138 **2.3 Elemental and isotopic analyses of POM**

139 Filters containing particulate matter were dried at  $45\text{ }^\circ\text{C}$  for 24 h, after which carbonates were  
140 removed by exposing the filters to fumes of 35% HCl for 6 h in a desiccator. The treated filters  
141 were then weighed and tightly packed into tin capsules for elemental and isotopic analyses (Jain  
142 et al., 2019; Singh et al., 2024b). Particulate nitrogen (PN), particulate organic carbon (POC),  $\delta^{13}\text{C}$ -  
143 POC, and  $\delta^{15}\text{N}$ -PN were measured at the Marine Stable Isotope Laboratory, National Centre for  
144 Polar and Ocean Research, Goa, India, using an elemental analyzer coupled to an isotope ratio  
145 mass spectrometer (EA-IRMS; Isoprime Vario Isotope Cube) operated in continuous-flow mode.  
146 External analytical precision for  $\delta^{13}\text{C}$  and  $\delta^{15}\text{N}$  was  $\pm 0.10\text{‰}$  and  $\pm 0.14\text{‰}$  ( $1\sigma$ ), respectively,  
147 determined by repeated analysis of caffeine (IAEA-600) and ammonium sulphate (IAEA-N1)  
148 standards.  $\delta^{13}\text{C}$  and  $\delta^{15}\text{N}$  values are reported relative to VPDB and Air- $\text{N}_2$ , respectively, with  
149 ammonium sulfate (IAEA-N1) used for normalization to Air- $\text{N}_2$ . External precision for  $\%C$  and  
150  $\%N$  was  $\pm 0.96\%$  and  $\pm 0.95\%$  ( $1\sigma$ ), respectively, based on repeated measurements of  
151 sulfanilamide.

## 152 **2.4 Biochemical analysis of POM**

153 The dried, pre-weighed filters with POM were cut into smaller pieces using clean stainless-steel  
154 scissors and then used for further analysis. The total particulate carbohydrates (P-CHO),  
155 particulate proteins (P-PRT), and particulate lipids (P-LIP) were analyzed using the phenol-  
156 sulfuric acid (Dubois et al., 1956), Lowry (Upreti et al., 1988), and Phospho-Vanillin (Folch et al.,  
157 1957) methods, respectively, and as described earlier in (Singh et al., 2024b). Biopolymeric carbon  
158 (BPC) was determined as depicted by (Danovaro et al., 2001), using the sum of the carbon  
159 equivalents of P-CHO, P-PRT, and P-LIP (conversion factors of 0.4, 0.49 and 0.75, respectively).

160

## 161 **2.5 Monosaccharide composition analysis of POM**

162 For monosaccharide analysis, POM samples were acid-hydrolyzed and then analyzed using High-  
163 Performance Anion Exchange Chromatography coupled with a Pulsed Amperometric Detector  
164 (HPAEC-PAD) as described earlier by (Singh et al., 2024a). In brief, GF/F filters with POM were  
165 treated with 1 mL of 12 M H<sub>2</sub>SO<sub>4</sub> at 25 °C for 2 h, diluted to 1.2 M with Milli-Q water, purged  
166 with N<sub>2</sub>, sealed, and incubated at 100 °C for 4 h. After cooling, the internal standard (myo-inositol)  
167 was added, and the samples were neutralized with pre-combusted CaCO<sub>3</sub>, centrifuged (6000 rpm,  
168 10 min), and filtered (0.22 µm PTFE). The samples were analyzed using HPAEC-PAD (Metrohm  
169 940 Professional IC Vario) equipped with an Au working electrode and Ag/AgCl reference  
170 electrode, on a Metrosep Carb 2 (250/4.0) coupled with a guard column at 30 °C. Sugars were  
171 separated using gradient elution (0.6 mL min<sup>-1</sup>) with solvent A (1 mM NaOH, 1 mM sodium  
172 acetate) and solvent B (150 mM NaOH, 100 mM sodium acetate) over 120 min. Neutral sugars,  
173 amino sugars, and mannitol were resolved isocratically with solvent A, while acidic sugars were

174 separated using a solvent B gradient. Identification and quantification of monosaccharides were  
175 achieved using calibration with a mixture of sugar standards (Sigma).

176

## 177 **2.6 Amino acid composition analysis of POM**

178 For amino acid analysis, POM samples were acid-hydrolyzed using HCl and then analyzed using  
179 High-Performance Liquid Chromatography coupled with a Diode Array Detector (HPLC-DAD)  
180 using the method outlined by (Kim et al., 2024). GF/F filters with POM were cut into small pieces,  
181 placed in Pyrex tubes with 10 mL of 6 M HCl, purged with N<sub>2</sub>, sealed, and hydrolyzed at 110 °C  
182 for 22 h. After cooling, nor-leucine was added as an internal standard. The hydrolysate was  
183 centrifuged, freeze-dried, reconstituted in 1 mL of Milli-Q water, vortexed, and filtered (0.22 μm).  
184 Amino acids were derivatized by sequentially mixing 2.5 μL borate buffer with 1 μL sample (0.5  
185 min), followed by addition of 1 μL OPA reagent, mixing, and dilution with 15.5 μL of Milli-Q  
186 water in the HPLC (Agilent 1200) autosampler prior to injection. HPLC separation of the  
187 derivatized amino acids was carried out using a Zorbax AAA column (5 μm, 4.6 × 150 mm), a 20  
188 μL injection volume, and a flow rate of 2 mL min<sup>-1</sup>. Detection was performed using a DAD  
189 (Agilent) at 338 nm (reference 390 nm). The separation was carried out using gradient elution with  
190 mobile phase A (40 mM phosphate buffer, pH 8.2) and mobile phase B (acetonitrile:  
191 methanol:water, 45:45:10). Identification and quantification were performed using external  
192 calibration with a 17 amino acid standard mixture (Fig. S1: 10, 100, 250, 1000 pmol, Agilent,  
193 USA).

194

## 195 **2.7 Statistical analysis**

196 Statistical analysis was performed using R (version 4.6.0), prior to Analysis of variance (ANOVA)  
197 the assumption for normality and homogeneity of variance were assessed using Shapiro-Wilk and  
198 Levene's test (Table S1). Pearson correlation analysis was performed at a significance level of  
199 0.05 to examine the relationship between the variables. Principal component analysis (PCA) was  
200 employed using the *vegan* and *factoextra* packages to visualize the biogeochemical gradient, and  
201 all plots were generated using *ggplot2*.

202

### 203 **3. Results**

#### 204 **3.1 Salinity, temperature, nutrients, and chl-a**

205 Surface seawater salinity exhibited spatial variation, with the lowest salinity ( $27.4 \pm 0.0$  psu)  
206 recorded at NA\_1500 station, a site most influenced by glacier meltwater, and the highest salinity  
207 ( $31.6 \pm 0.1$  psu) observed at KN\_MDS, the outermost site under the influence of oceanic circulation  
208 (Table 1). Surface seawater temperature was lowest ( $4.2 \pm 0.0$  °C) at NA\_500 and highest at  
209 KN\_MDS ( $5.5 \pm 0.0$  °C). The lowest turbidity ( $2.1 \pm 0.1$  NTU) was recorded at both BD\_MDS and  
210 HN\_MDS, while maximum turbidity ( $7.4 \pm 0.0$  NTU) was observed at KN\_MDS.

211 Nitrate varied from  $0.05$   $\mu\text{M}$  (BD\_MDS) to  $0.80$   $\mu\text{M}$  (NA\_1500) and showed an increasing  
212 trend from MDS to Adj-W for NA, BD, and HN (Table 1). The overall average nitrate  
213 concentrations were lower in MDS ( $0.39 \pm 0.23$   $\mu\text{M}$ ) than in Adj-W ( $0.56 \pm 0.13$   $\mu\text{M}$ ). Comparing  
214 different stations, the average nitrate concentration of all NA stations were high ( $0.66 \pm 0.12$   $\mu\text{M}$ ),  
215 followed by KN ( $0.53 \pm 0.10$   $\mu\text{M}$ ), HN ( $0.51 \pm 0.08$   $\mu\text{M}$ ), and lowest at BD stations ( $0.30 \pm 0.22$   $\mu\text{M}$ ).  
216 Nitrite concentration showed a similar pattern, with an increasing trend from MDS to Adj-W sites.  
217 However, phosphate concentrations showed minor differences ( $0.01$  to  $0.02$   $\mu\text{M}$ ) among MDS and  
218 Adj-W sites.

219 Chlorophyll *a* (Chl *a*) concentrations ranged from 0.04  $\mu\text{g L}^{-1}$  to 0.18  $\mu\text{g L}^{-1}$  across all  
 220 stations (Table 1) and with no clear trend in other photosynthetic pigments (Table S2). Similar to  
 221 nitrate, Chl *a* showed an increasing trend from MDS to Adj-W sites at the NA, BD, and HN  
 222 stations, while KN exhibited relatively low concentrations at both MDS and Adj-W sites. Overall,  
 223 the average Chl *a* concentration was lower at MDS (0.07  $\mu\text{g L}^{-1}$ ) compared to Adj-W (0.08  $\mu\text{g}$   
 224  $\text{L}^{-1}$ ). Among stations, BD stations recorded the highest average Chl *a* concentrations (0.11  $\mu\text{g L}^{-1}$ ),  
 225 followed by HN and NA with 0.07  $\mu\text{g L}^{-1}$ , whereas KN (0.04  $\mu\text{g L}^{-1}$ ) stations exhibited the lowest  
 226 average concentrations.

227  
 228 **Table 1.** Sampling stations and measured physicochemical parameters (temperature, salinity,  
 229 nutrients, and chlorophyll *a*) across sampling stations.

Station	Station depth [m]	Temperature [°C]	Salinity [PSU]	Turbidity [NTU]	Nitrate ( $\mu\text{M}$ )	Phosphate ( $\mu\text{M}$ )	Nitrite ( $\mu\text{M}$ )	Chlorophyll <i>a</i> [ $\mu\text{g L}^{-1}$ ]
NA_MDS	3.5	5.0±0.1	31.3±0.0	3.5±0.4	0.58	0.18	0.09	0.09
NA_500	122	4.2±0.0	30.1±1.3	5.0±0.1	0.61	0.17	0.11	0.04
NA_1500	300	5.2±0.1	27.4±0.0	2.9±0.4	0.80	0.20	0.11	0.08
BD_MDS	6.7	5.1±0.0	29.9±0.0	2.1±0.1	0.05	0.13	0.01	0.09
BD_500	146	4.7±0.3	30.3±0.1	2.9±0.1	0.39	0.15	0.04	0.18
BD_1500	362	5.4±0.0	30.9±0.6	4.4±0.3	0.45	0.15	0.06	0.05
KN_MDS	3.4	5.5±0.0	31.6±0.1	7.4±0.0	0.49	0.14	0.06	0.05
KN_500	216	5.0±0.5	29.5±0.1	3.1±0.4	0.65	0.16	0.08	0.06
KN_1500	240	4.5±0.0	29.8±0.0	2.9±0.1	0.45	0.14	0.07	0.05
HN_MDS	4.5	4.5±0.2	28.7±1.8	2.1±0.1	0.43	0.14	0.04	0.06
HN_500	76	4.3±0.0	29.8±0.0	3.8±1.7	0.58	0.13	0.05	0.06
HN_1500	315	4.3±0.0	29.8±0.3	3.8±0.5	0.52	0.13	0.07	0.09

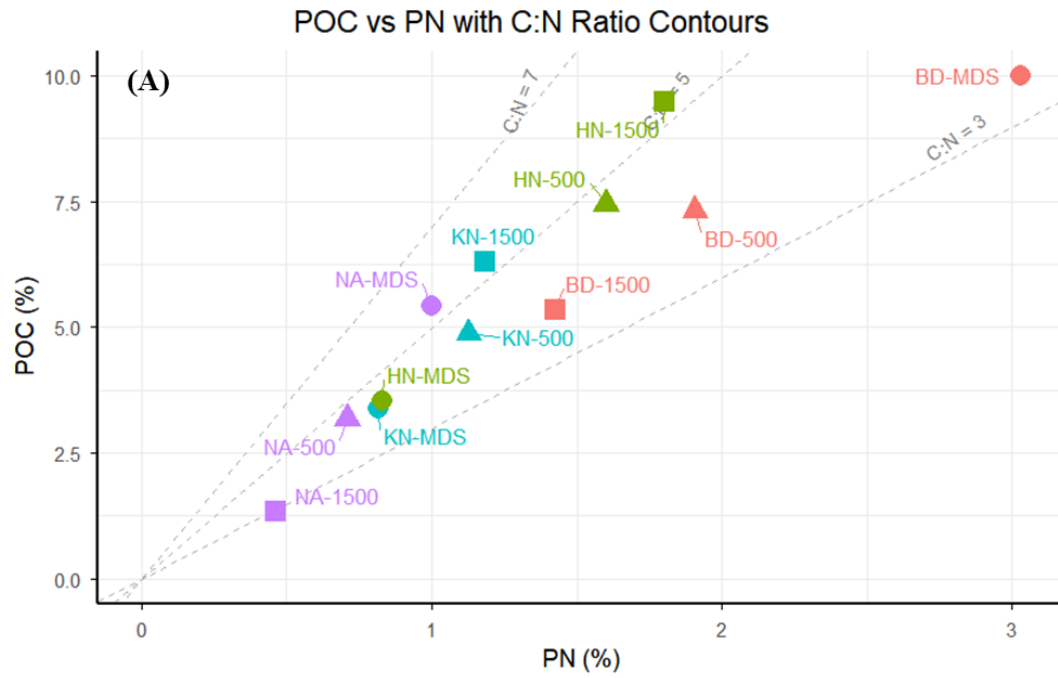
230

231

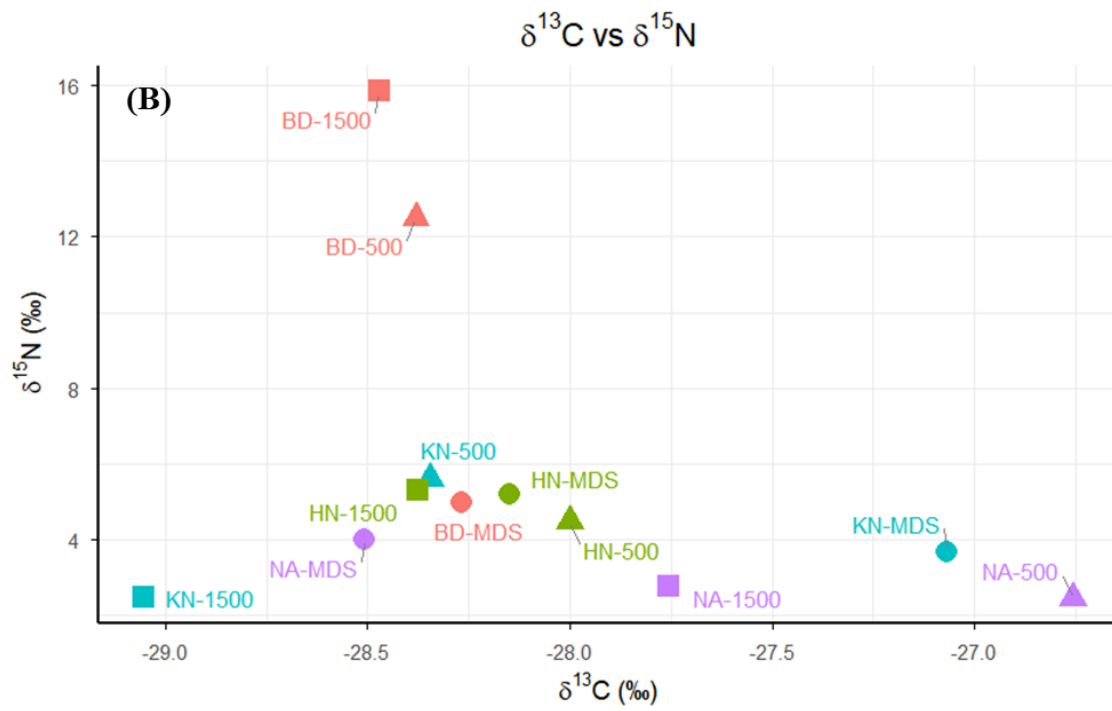
### 232 3.2 Elemental and stable isotopic composition

233 POC and PN concentrations varied over a wide range from 0.17 mg L<sup>-1</sup> (KN\_500) to 0.45 mg L<sup>-1</sup>  
234 (BD\_MDS) and from 0.04 mg L<sup>-1</sup> (KN\_500 and KN\_1500) to 0.14 mg L<sup>-1</sup> (BD\_MDS),  
235 respectively (Fig. 2A). BD\_MDS recorded the highest POC concentration (0.45 mg L<sup>-1</sup>), followed  
236 by NA\_MDS and HN\_MDS (0.32 mg L<sup>-1</sup>), with the lowest POC at KN\_MDS (0.21 mg L<sup>-1</sup>).  
237 Overall average POC and PN concentrations were higher at MDS (0.32±0.10 and 0.08±0.04 mg  
238 L<sup>-1</sup>, respectively) than at Adj-W (0.26±0.08 and 0.06±0.02 mg L<sup>-1</sup>), respectively. Across stations,  
239 mean POC was highest at BD (0.37±0.10 mg L<sup>-1</sup>), followed by HN (0.32±0.01 mg L<sup>-1</sup>) and NA  
240 (0.24±0.07 mg L<sup>-1</sup>), and lowest at KN (0.19±0.02 mg L<sup>-1</sup>) (Fig. 2B). A similar pattern was  
241 observed for PN, with the highest values at BD (0.10 ± 0.03 mg L<sup>-1</sup>), followed by HN (0.07±0.01  
242 mg L<sup>-1</sup>), NA (0.06±0.00 mg L<sup>-1</sup>), and KN (0.04±0.01 mg L<sup>-1</sup>). The POC/PN ratio ranged from 2.9  
243 (NA\_1500) to 5.4 (NA\_MDS). The POC/PN ratio showed an increasing trend from MDS to Adj-  
244 W for all stations, except NA (Fig. 2C). The NA station showed a decreasing trend in POC/PN  
245 ratio from MDS (5.4) to Adj-W (2.9) with the highest change of 2.5.

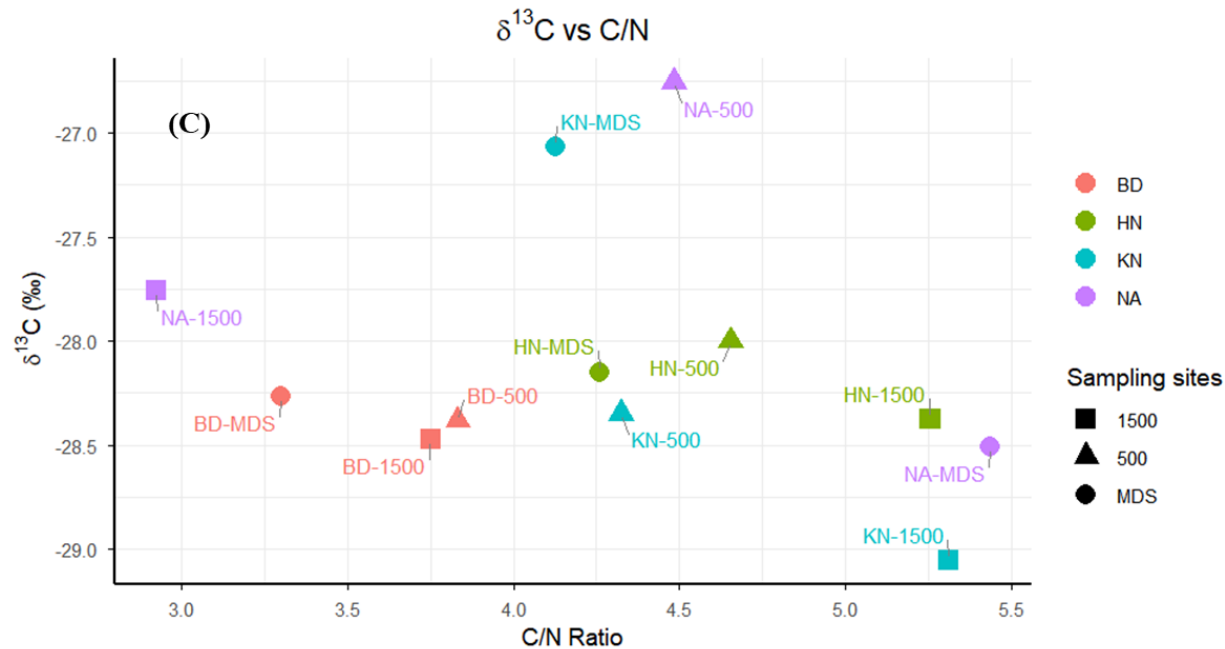
246 The  $\delta^{13}\text{C}$  and  $\delta^{15}\text{N}$  values of POM varied from -26.8‰ (NA\_500) to -29.1‰ (KN\_1500)  
247 and from 2.5 (KN\_1500) to 15.9 (BD\_1500), respectively. Mean  $\delta^{13}\text{C}$  values of all MDS stations  
248 (-28.0±0.64‰) were similar to those of Adj-W stations (-28.1±0.67‰). However, individually,  
249 KN showed a prominent decreasing trend in  $\delta^{13}\text{C}$  (-27.1‰ to -29.1‰) and NA showed an increase  
250 of -28.5‰ to -27.5‰ from MDS to Adj-W, while HN and BD values were confined to a narrow  
251 range (-28.0‰ to -28.5‰). For  $\delta^{15}\text{N}$ , the overall average at MDS sites was lower (4.5 ± 0.73‰)  
252 than at Adj-W (6.4 ± 5.02‰).  $\delta^{15}\text{N}$  value variations were minor (2.5‰ to 5.6‰) for the KN, HN,  
253 and NA stations, while the observed values for BD\_500 (12.5‰) and BD\_1500 (15.9‰) were  
254 quite high (Fig. 2B).



255



256



257  
 258 **Figure 2.** Relationship between Particulate Organic Carbon (POC %) and Particulate Nitrogen  
 259 (PN %) relative to C/N ratio contours (A), dual isotope plot of  $\delta^{13}\text{C}$  and  $\delta^{15}\text{N}$  signatures (B) and  
 260  $\delta^{13}\text{C}$  versus C/N ratio in particulate organic matter (C)

261  
 262 **3.3 Biochemical and biomolecular composition of POM**

263 *3.3.1 Concentrations of carbohydrates, proteins, and lipids*

264 Particulate carbohydrate (PCHO) and proteins (PPRT) concentrations showed a decreasing trend  
 265 from MDS (PCHO: 55.7 to 109.7  $\mu\text{g L}^{-1}$ ; PRT: 56.7 to 145.5  $\mu\text{g L}^{-1}$ ) to Adj-W (PCHO: 46.2 to  
 266 84.6  $\mu\text{g L}^{-1}$ ; PPRT: 32.1 to 94.4  $\mu\text{g L}^{-1}$ ) for all stations (Table 2). Unlike PCHO and PPRT,  
 267 particulate lipids (PLIP) concentrations showed an increasing trend from MDS to Adj-W for NA  
 268 (59.6  $\mu\text{g L}^{-1}$  to 106.7  $\mu\text{g L}^{-1}$ ) and KN (51.6  $\mu\text{g L}^{-1}$  to 70.9  $\mu\text{g L}^{-1}$ ), and a decreasing trend for BD  
 269 (122.7  $\mu\text{g L}^{-1}$  to 83.3  $\mu\text{g L}^{-1}$ ). For HN stations, HN\_500 (118.1  $\mu\text{g L}^{-1}$ ) showed the highest PLIP  
 270 concentrations, followed by HN\_MDS (77.8  $\mu\text{g L}^{-1}$ ) and HN\_1500 (47.5  $\mu\text{g L}^{-1}$ ). Among stations,

271 BD stations showed the highest average PCHO (90.7  $\mu\text{g L}^{-1}$ ), PPRT (105.4  $\mu\text{g L}^{-1}$ ), and PLIP  
 272 (105.4  $\mu\text{g L}^{-1}$ ) concentrations.

273

274 **Table 2.** Concentrations of particulate biochemical components, including carbohydrates (P-  
 275 CHO), proteins (P-PRT), and lipids (P-LIP), alongside their biopolymeric carbon equivalents  
 276 (BPC-CHO, BPC-PRT, BPC-LIP) and total biopolymeric carbon (BPC) across the sampling  
 277 stations.

Station	P-CHO ( $\mu\text{g L}^{-1}$ )	P-PRT ( $\mu\text{g L}^{-1}$ )	P-LIP ( $\mu\text{g L}^{-1}$ )	BPC-CHO ( $\mu\text{g L}^{-1}$ )	BPC-PRT ( $\mu\text{g L}^{-1}$ )	BPC-LIP ( $\mu\text{g L}^{-1}$ )	BPC (%)	BPC/POC (%)	Labile (%)
NA_MDS	67.7	61.1	59.6	27.1	29.9	44.7	31.7	31.7	17.8
NA_500	54.9	45.5	67.7	22.0	22.3	50.8	45.1	45.1	21.0
NA_1500	46.2	32.1	106.7	18.5	15.7	80.0	60.0	60.0	18.0
BD_MDS	109.7	145.5	122.7	43.9	71.3	92.0	46.3	46.3	25.7
BD_500	84.6	94.4	110.3	33.8	46.3	82.7	40.0	40.0	19.7
BD_1500	77.8	64.2	83.3	31.1	31.5	62.4	47.7	47.7	23.9
KN_MDS	55.7	56.7	51.6	22.3	27.8	38.7	42.2	42.2	23.8
KN_500	46.8	42.6	51.9	18.7	20.9	38.9	46.9	46.9	23.7
KN_1500	53.4	39.1	70.9	21.4	19.2	53.1	50.1	50.1	21.7
HN_MDS	78.6	97.0	77.8	31.4	47.5	58.3	43.4	43.4	25.0
HN_500	75.3	86.2	118.1	30.1	42.2	88.6	49.5	49.5	22.2
HN_1500	73.7	81.8	47.5	29.5	40.1	35.6	33.5	33.5	22.2

278 BPC\_CHO: Biopolymeric carbon equivalent carbohydrate; BPC\_PRT: Carbon equivalent bio-  
 279 polymeric protein; BPC\_LIP: Carbon equivalent bio-polymeric lipid

280

281 *3.3.2 Biopolymeric vs. Non-Biopolymeric Carbon in POM*

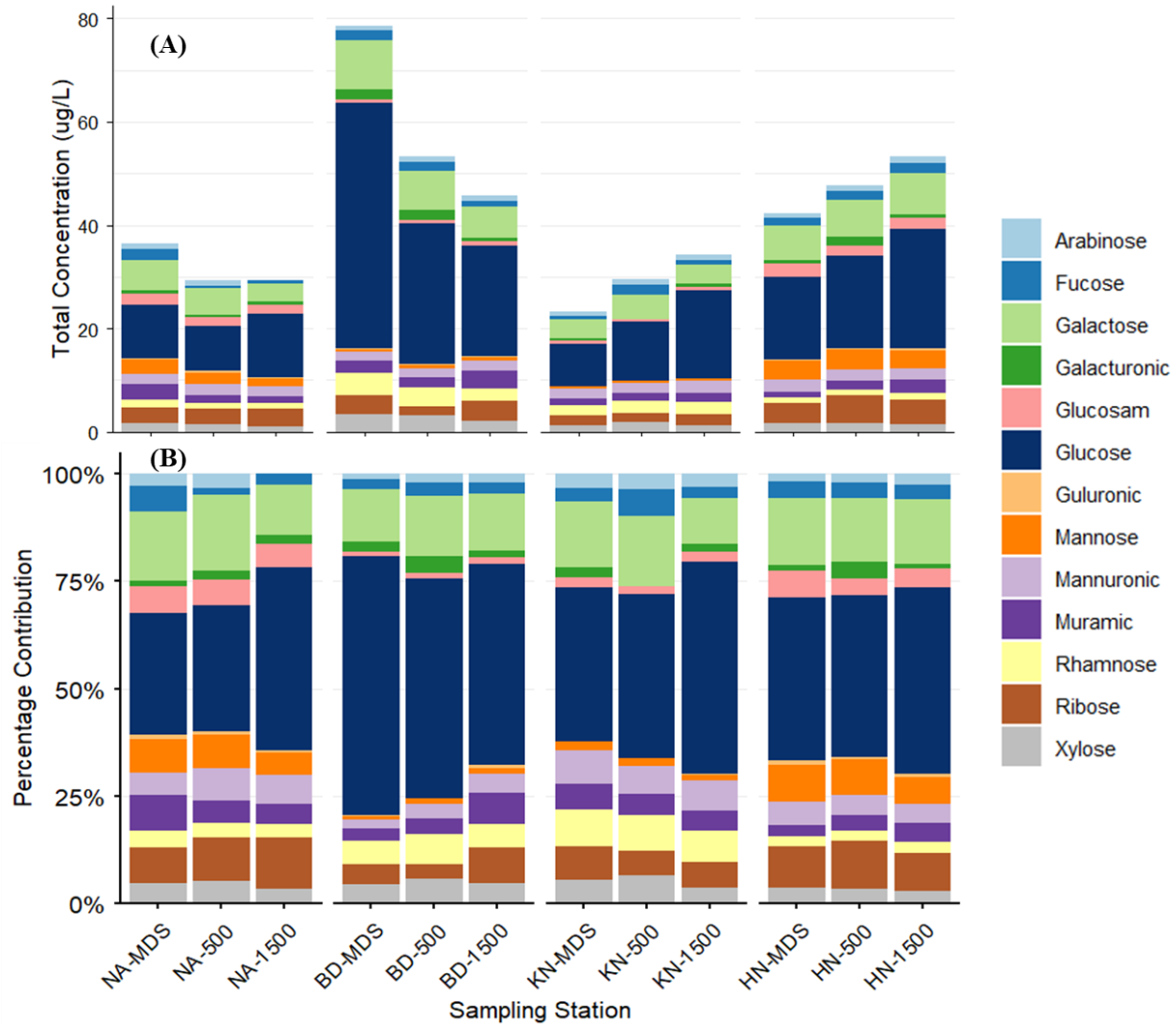
282 A consistent increase in BPC (%) from MDS to Adj-W was observed at NA and KN (Table 2 and  
283 Table S3). In contrast, BD exhibited lower BPC at BD\_500 compared to both BD\_MDS and  
284 BD\_1500 (Table 2). For HN, BPC% was highest at HN\_500 compared to HN\_MDS and  
285 HN\_1500. Overall, BPC\_CHO and BPC\_PPRT, representing labile components of POC, showed  
286 a consistent difference of 2-6% between MDS and Adj-W at individual sampling stations. The  
287 most significant variation occurred at BD sites, with BD\_500 showing 19.6% of labile component  
288 contributions, followed by BD\_1500 (23.9%) and BD\_MDS (25.7%).

289

### 290 3.3.3 Monosaccharide composition of POM

291 Total monosaccharide concentrations at NA and BD declined from MDS to Adj-W (Fig. 3A and  
292 Table S3). In contrast, KN and HN exhibited increasing monosaccharide concentrations from  
293 MDS to Adj-W. Glucose (8.6 - 47.5  $\mu\text{g L}^{-1}$ ) and galactose (3.4 - 9.6  $\mu\text{g L}^{-1}$ ) dominated the  
294 monosaccharide pool and followed trends similar to total monosaccharides from MDS to Adj-W  
295 across stations. Station-wise, average monosaccharide concentrations were highest at BD (59.2  $\mu\text{g}$   
296  $\text{L}^{-1}$ ), followed by HN (47.9  $\mu\text{g L}^{-1}$ ), NA (32.0  $\mu\text{g L}^{-1}$ ), and KN (29.0  $\mu\text{g L}^{-1}$ ).

297 The mol% monosaccharide concentrations showed a consistent pattern across MDS and  
298 Adj-W for each station, with minor differences (Fig. 3B). However, BD and KN stations showed  
299 different compositions compared to NA and HN stations, mainly due to the contributions of  
300 glucosamine and rhamnose. Glucose, the dominant monosaccharide, exhibited a decreasing mol%  
301 trend from MDS to Adj-W at the BD station, whereas it showed an increasing mol% trend offshore  
302 at the other stations.



303

304 **Figure 3.** Spatial variation in monosaccharide composition of surface POM across fjord stations.

305 (A) Concentrations ( $\mu\text{g L}^{-1}$ ) and (B) relative percentage contributions of individual

306 monosaccharides at macroalgal bed (MDS), 500 m, and 1500 m sites at NA, BD, KN, and HN.

307

### 308 3.3.4 Amino acid composition of POM

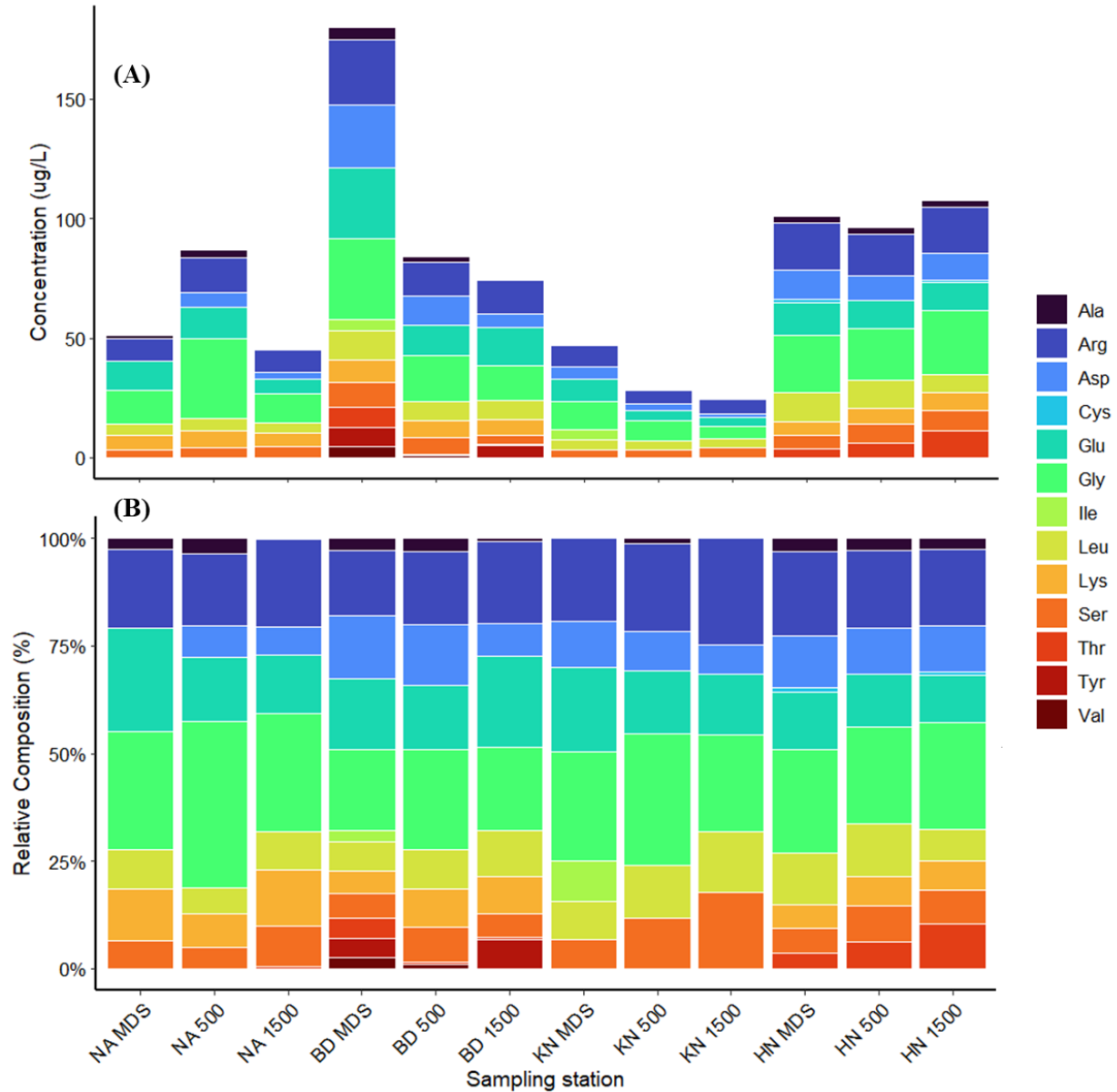
309 A clear decreasing trend in total amino acid concentrations from MDS to Adj-W was observed at

310 BD and KN (Fig. 4A and Table S3). In contrast, concentrations at NA increased from NA\_MDS

311 to NA\_500 further declined at NA\_1500. At HN, total amino acid concentrations decreased

312 slightly from HN\_MDS to HN\_500 and then increased at HN\_1500. Among stations, the average  
313 total amino acid concentrations were highest at BD (113  $\mu\text{g L}^{-1}$ ) followed by HN (101.6  $\mu\text{g L}^{-1}$ ),  
314 NA (61  $\mu\text{g L}^{-1}$ ) and KN (33.3  $\mu\text{g L}^{-1}$ ), also the average individual amino acid concentration were  
315 high in MDS than Adj-W (Table S4). The BD station showed the highest concentrations of  
316 individual amino acids, with Asp (26.1  $\mu\text{g L}^{-1}$ ), Glu (29.8  $\mu\text{g L}^{-1}$ ), Gly (33.9  $\mu\text{g L}^{-1}$ ), Arg (27.6  $\mu\text{g}$   
317  $\text{L}^{-1}$ ), and Lys (9.4  $\mu\text{g L}^{-1}$ ) peaking at the MDS and declining toward Adj-W (Asp: 5.6  $\mu\text{g L}^{-1}$ ; Glu:  
318 15.9  $\mu\text{g L}^{-1}$ ; Gly: 14.4  $\mu\text{g L}^{-1}$ ; Arg: 14.4  $\mu\text{g L}^{-1}$ ; Lys: 6.5  $\mu\text{g L}^{-1}$ ). A similar decreasing pattern of  
319 the individual amino acids was observed for the KN station. Exceptions to the low individual  
320 amino acid concentrations at Adj-W (500 and 1500 m locations) included high Gly at NA\_500  
321 (33.5  $\mu\text{g L}^{-1}$ ), and high Gly (26.7  $\mu\text{g L}^{-1}$ ) and Arg (19.1  $\mu\text{g L}^{-1}$ ) at HN\_1500.

322 Mol% concentrations of different amino acids indicated that Gly, Glu, and Arg were the  
323 dominant contributors across all sampling stations (Fig. 4B). The mol% concentration of Glu  
324 showed a decreasing trend from MDS to Adj-W at NA (24.1 % to 13.7%), KN (19.7% to 14.0%)  
325 and HN (13.3% to 10.9%) stations, whereas BD showed an increasing trend (MDS: 16.6%; Adj-  
326 W: 21.3%). In contrast, Gly and Arg exhibited similar spatial patterns across stations, with Gly  
327 showing its highest mol% contribution at the 500 m station at NA, BD, and KN, while Arg  
328 displayed a consistent increase from MDS to Adj-W across these stations.



329

330 **Figure 4.** Spatial variation in amino acid composition of surface POM across fjord stations. (A)

331 Concentrations ( $\mu\text{g L}^{-1}$ ) and (B) relative percentage contributions of individual amino acids at

332 macroalgal beds (MDS), 500 m and 1500 m sites in NA, BD, KN, and HN.

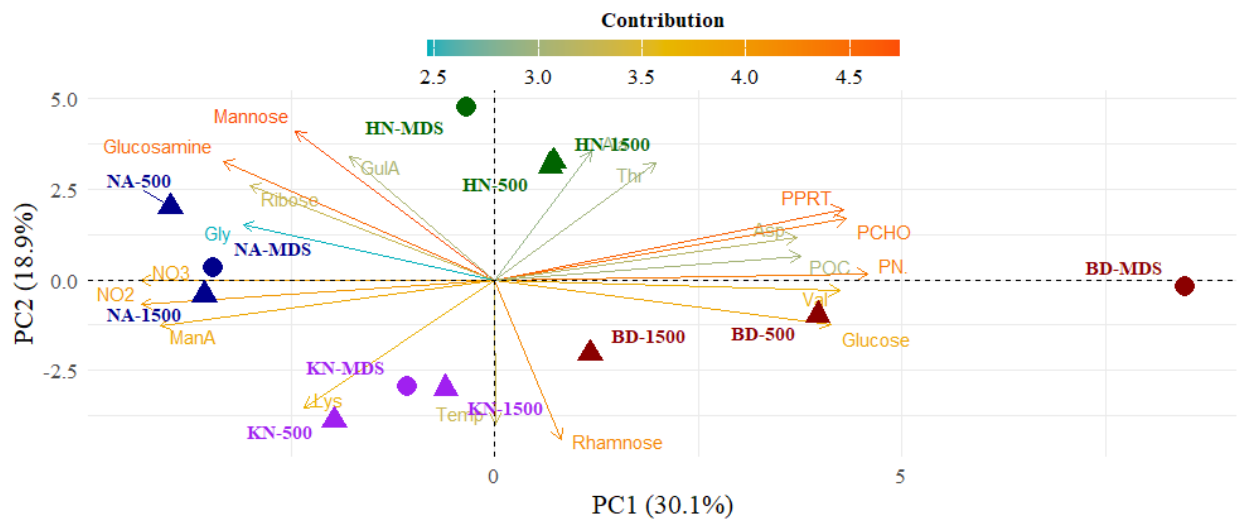
333

334 **3.4 Statistical analysis**

335 Strong positive correlations were observed between PN and POC, PCHO, and PPRT ( $r > 0.83$ ,  
336  $p < 0.05$ ), with an exceptionally high correlation between PPRT and PCHO ( $r = 0.96$ ,  $p < 0.05$ ) (Fig.  
337 S2A). In contrast, negative correlations were observed between BPC\_LIP% and the non-BPC  
338 fraction ( $r = -0.95$ ,  $p < 0.05$ ), and between nitrate and biochemical parameters (POC, PN, PCHO,  
339 PPRT) ( $r < -0.66$ ,  $p < 0.05$ ). Despite consistent trends across parameters, ANOVA indicated no  
340 significant differences between MDS and Adj-W, suggesting gradual lateral transformations rather  
341 than abrupt distance-related changes, together with pronounced spatial heterogeneity among  
342 stations (Table S1).

343 Mannuronic acid (ManA) showed strong negative correlations with POC ( $r = -0.79$ ) and  
344 PCHO ( $r = -0.92$ ) (Fig. S2B). Glucose and galactose were negatively correlated with several  
345 compounds, including glucosamine ( $r = -0.72$ ), mannose ( $r = -0.70$ ), ribose ( $r = -0.59$ ), and ManA  
346 ( $r = -0.63$ ). Rhamnose exhibited pronounced negative relationships with guluronic acid (GulA;  $r$   
347  $= -0.83$ ), glucosamine ( $r = -0.76$ ), mannose ( $r = -0.85$ ), and ribose ( $r = -0.73$ ), whereas galactose  
348 was positively correlated with fructose ( $r = 0.61$ ) and arabinose ( $r = 0.58$ ). Strong positive  
349 associations were also observed among mannose, glucosamine ( $r = 0.91$ ), and ribose ( $r = 0.76$ ),  
350 with ribose additionally correlating positively with glucosamine ( $r = 0.79$ ).

351 In PCA, the first two principal components explained 49.0% of the total variance, with PC1  
352 and PC2 accounting for 30.1% and 18.9%, respectively (Fig. 5). PC1 was positively loaded by  
353 POC, PN, PCHO, PPRT, glucose, galactose, and labile amino acids (Asp, Glu, Thr), whereas  
354 negative PC1 loadings were associated with muramic acid, arabinose, fucose, and inorganic  
355 nutrients. Sample scores showed a spatial organization, with MDS plotting toward positive PC1  
356 values and Adj-W progressively shifting toward negative PC1 values, which was seen more  
357 prominently for BD stations.

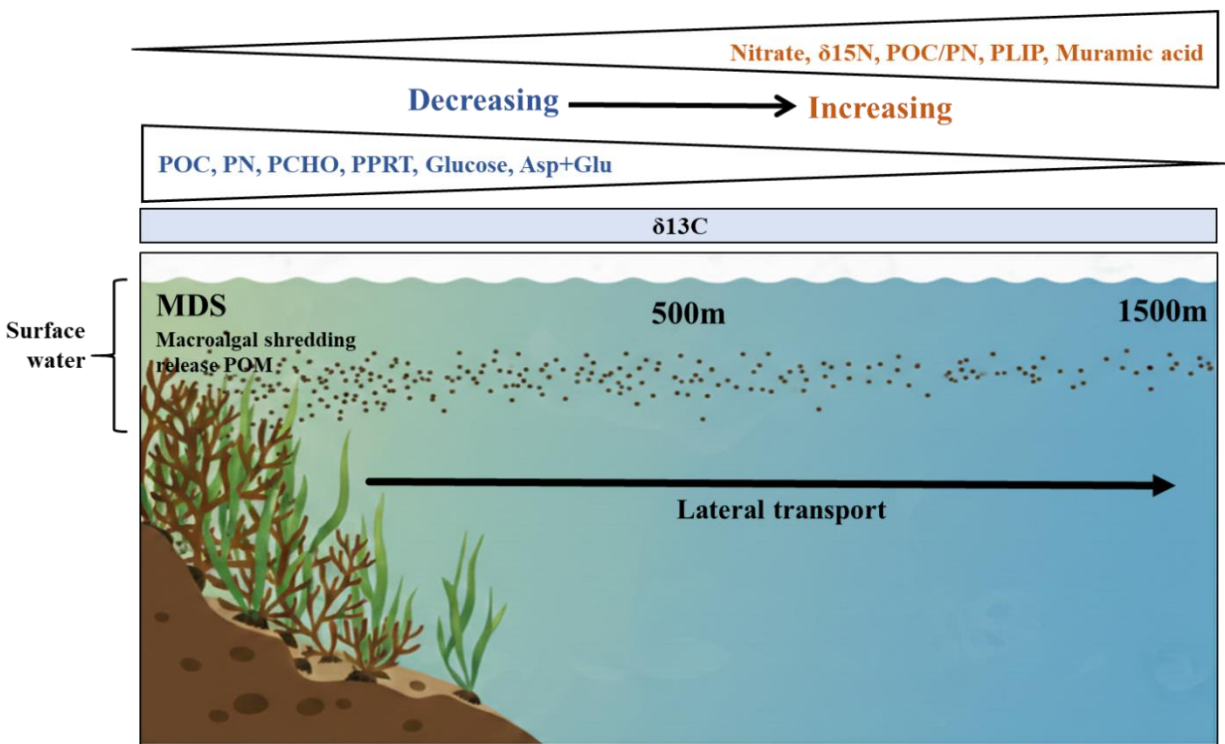


358  
 359 **Figure 5.** Principal Component Analysis (PCA) biplot of biogeochemical variables across  
 360 different sample sites. The first two principal components (PC1 and PC2) account for 30.1% and  
 361 18.9% of the total variance, respectively. Individual samples are represented by colored shapes,  
 362 categorized by site (e.g., NA, HN, KN, BD) and location (e.g., MDS, 500, 1500). Vectors (arrows)  
 363 indicate the loadings of specific variables, including carbohydrates (e.g., Mannose, Glucose,  
 364 Rhamnose), nutrients ( $\text{NO}_2^-$ ,  $\text{NO}_3^-$ ), and organic matter indicators (POC, PN, PCHO, PPRT). The  
 365 color scale of the vectors represents the contribution of each variable to the principal components.

366  
 367 **4. Discussion**

368 The present study provides a multi-proxy assessment of POM in the surface waters of macroalgal  
 369 beds in Kongsfjorden, integrating bulk biochemical, isotopic, biopolymeric composition, and  
 370 molecular biomarkers. Elevated bulk (POC, PN, PCHO, and PPRT) and molecular  
 371 (monosaccharides and amino acids) concentrations at MDS indicated that macroalgal  
 372 localized sources of biochemically labile organic matter. The results demonstrated that macroalgal

373 beds imprint surface waters with distinct biochemical and molecular signatures that are  
 374 redistributed across fjord-scale gradients. The PCA demonstrates that macroalgae influence  
 375 surface POM along a continuous multivariate gradient rather than discrete habitat classes. The  
 376 systematic offshore decline of these compounds, together with internal reorganization of the  
 377 biopolymeric and molecular composition, shows that macroalgal-derived POM is efficiently  
 378 exported and selectively transformed during lateral transport (Fig. 6).



379  
 380 **Figure 6.** Schematic showing the biochemical nature of POM at macroalgal dominated sites and  
 381 its transformation during lateral transport.

382  
 383 **4.1 Influence of Macroalgal Beds on Surface POM Biochemical Composition**  
 384 Macroalgal beds produce substantial organic carbon via photosynthesis, which enters surrounding  
 385 waters (Chen et al., 2020; Filbee-Dexter et al., 2022; Pessarrodona et al., 2022; Watanabe et al.,

386 2020). The observed higher concentrations of POC and PN at MDS relative to Adj-W, together  
387 with consistently higher PCHO and PPRT, indicated localized enrichment of particulate matter  
388 near macroalgal beds. The inverse relationship of nitrate with POC, PN, PCHO, and PPRT ( $r =$   
389  $-0.82$ ,  $p < 0.05$ ) reflects biological assimilation of dissolved nutrients into the particulate pool,  
390 reinforcing the role of active coastal production in shaping POM composition along the fjord  
391 gradient. Macroalgal tissues are structurally rich in polysaccharides and contain substantial protein  
392 fractions, and the release of tissue fragments, sloughed material, and epiphyte-associated biomass  
393 (Kennedy and Blain, 2025; Watanabe et al., 2020) provides a direct pathway for incorporation of  
394 macroalgal carbon into surface POM contributing to Arctic coastal carbon cycling (Ager et al.,  
395 2023). Strong positive correlations ( $r > 0.83$ ,  $p < 0.05$ ) between PN and POC, PCHO, and PPRT  
396 indicate tightly coupled carbon and nitrogen incorporation during fresh organic matter production.  
397 The remarkably strong positive correlation between PPRT and PCHO ( $r = 0.96$ ,  $p < 0.05$ ) further  
398 indicates tightly coupled biological production and POM synthesis in macroalgal beds. The  
399 multivariate analysis of POM as resolved by PCA showed PC1 (30.1% variance) was dominated  
400 by PCHO, PPRT, PN, POC, glucose, and Asp and separated MDS from Adj-W along a continuous  
401 biochemical gradient, especially prominent for BD station (Fig. 5). The strong positive loadings  
402 of labile carbon and nitrogen compounds supported a distinct organic-rich biochemical state of  
403 surface POM at MDS.

404         Although macroalgal biomass and detritus are generally carbon-rich, three of the four  
405 stations (BD, KN, and HN) exhibited lower POC/PN ratios at the MDS sites than Adj-W. This  
406 pattern likely reflects contributions from fresh, nitrogen-rich organic matter produced within  
407 macroalgal habitats, possibly including phytoplankton, epiphytic microalgae, and benthic primary  
408 producers associated with kelp beds (Burfeid-Castellanos et al., 2021; Stanca and Parsons, 2021),

409 which could be re-suspended into surface waters and become part of POM. Kelp forest POM  
410 characteristics are highly variable depending on the water column conditions, which also influence  
411 contributions from macroalgal detritus and other autochthonous primary producers (Dyer et al.,  
412 2019). In favorable conditions, other primary producers may outweigh the stoichiometric signal of  
413 macroalgal tissue itself, resulting in relatively low POC/PN ratios of POM near macroalgal beds  
414 (Chen et al., 2020). Similarly, heterotrophic bacteria are typically richer in nitrogen and  
415 phosphorus than phytoplankton, and their colonization of particles can lower the bulk POC/PN  
416 ratio by contributing N-rich biomass (Jo et al., 2021). The subsequent increase in POC/PN ratios  
417 from MDS to Adj-W is consistent with preferential microbial degradation of labile nitrogen-rich  
418 compounds during lateral transport (Vidal et al., 2018), leading to relative enrichment of carbon-  
419 rich material with distance from source habitats.

420  $\delta^{13}\text{C}$  values of POM are widely used to trace organic matter sources (Gao et al., 2008;  
421 Pineault et al., 2013). Most macroalgae typically exhibit  $\delta^{13}\text{C}$  values between  $-34.6\text{‰}$  to  $-2.2\text{‰}$   
422 (Velázquez-Ochoa et al., 2022), though some brown macroalgal species show more negative  
423 signatures, ranging from  $-20\text{‰}$  to  $-35\text{‰}$  (Fredriksen, 2003). In Arctic coastal systems, marine  
424 phytoplankton-derived organic matter typically exhibits  $\delta^{13}\text{C}$  values between  $-20\text{‰}$  and  $-26\text{‰}$ ,  
425 whereas terrestrial organic matter derived from C3 vegetation is generally more depleted, around  
426  $-26\text{‰}$  to  $-29\text{‰}$  (Gao et al., 2008; Pineault et al., 2013). However, substantial overlap between  
427 marine and terrestrial isotopic ranges complicates source discrimination in Arctic fjord systems  
428 (Singh et al., 2024b). The similarity of  $\delta^{13}\text{C}$  values between MDS and Adj-W indicates that  
429 macroalgal material does not dominate bulk POM isotopically; instead, it contributes substantially  
430 within a mixed particulate pool of macroalgal, phytoplanktonic, and terrestrial organic matter in  
431 Arctic fjords (Ørberg et al., 2023; Roy et al., 2025). This muted isotopic signal likely reflects that

432 macroalgal influence on surface POM is not solely derived from detached kelp tissue, but is also  
433 mediated by contributions from epiphytic and benthic microalgal production (Burfeid-Castellanos  
434 et al., 2021; Stanca and Parsons, 2021) and biochemically distinct macroalgal fractions, whose  
435  $\delta^{13}\text{C}$  values overlap those of pelagic organic matter.

436  $\delta^{15}\text{N}$  values of POM exceeding  $\sim 2\text{‰}$  as observed in this study are consistent with marine  
437 nitrate-based production and microbial reworking, rather than atmospheric or  $\text{N}_2$ -fixation sources  
438 (Kuzyk et al., 2010), where intense benthic–pelagic coupling and rapid recycling of dissolved  
439 inorganic nitrogen promote isotopic enrichment of the available nitrogen pool (Elliott Smith and  
440 Fox, 2022). Reflecting the pattern more prominently,  $\delta^{15}\text{N}$  value at BD\_MDS ( $5.0\text{‰}$ ), which was  
441 already high, further increased toward Adj-W (BD\_500:  $12.5\text{‰}$ , BD\_1500:  $15.9\text{‰}$ ), indicating  
442 relatively fresher marine-derived organic matter within the macroalgal beds, which is transformed  
443 into relatively higher trophic contributions in surrounding waters.

444

#### 445 **4.2 Transformation of surface POM during lateral transport from macroalgal beds** 446 **to adjacent waters**

447 The biochemical composition of POM provides valuable insights into the nature of organic carbon  
448 and its benthic-pelagic coupling in macroalgal beds (Elliott Smith and Fox, 2022; Renaud et al.,  
449 2015). The observed systematic offshore changes in POM composition revealed both lateral  
450 transport and early transformation of macroalgal beds derived particles across the fjord (Vidal et  
451 al., 2018). The concentrations of PCHO and PPRT declined consistently from MDS to Adj-W,  
452 indicating progressive dilution of organic matter with distance sourced from macroalgal beds and  
453 associated autochthonous production (Ørberg et al., 2023; Smale et al., 2022; Simpkins et al.,  
454 2025). These labile compounds are preferentially consumed by particle-associated and free-living

455 microbes (Jain et al., 2019), serving as indicators of freshly produced, easily degradable organic  
456 matter (Li et al., 2025). In contrast, PLIP generally increased offshore (except at BD), indicating  
457 a relative enrichment of lipid-rich pelagic material and/or the preferential preservation of more  
458 stable lipid compounds during transport. This pattern likely reflects selective microbial  
459 degradation of labile carbohydrates and proteins during lateral transport, combined with mixing  
460 with newly produced pelagic material (Li et al., 2025), highlighting dynamic compositional  
461 transformation of POM from MDS to Adj-W.

462         The compositional shift in POM was further supported by changes observed in BPC  
463 fractions. BPC represents the labile fraction of POM, mainly comprising proteins, carbohydrates,  
464 and a lipid fraction, whereas the non-BPC fraction includes more refractory components such as  
465 lignin, humic substances, black carbon, and cellulose (Fabiano et al., 1993; Lobbes et al., 2000;  
466 Tselepides et al., 2000). Among BPC constituents, %BPC\_lipid increased markedly from MDS  
467 ( $17.8 \pm 2.8\%$ ) to Adj-W ( $25.1 \pm 8.6\%$ ), whereas the labile fraction (proteins and carbohydrates)  
468 showed minor differences between MDS ( $23.1 \pm 3.6\%$ ) and Adj-W ( $21.5 \pm 2.5\%$ ). This pattern  
469 suggests a relative enrichment of more stable organic matter within POC, accompanied by lateral  
470 degradation of labile components, consistent with the observed decline in POC from MDS to Adj-  
471 W. Further, the strong inverse relationship between %BPC\_LIP and the non-BPC fraction ( $r =$   
472  $-0.95$ ,  $p < 0.05$ ) suggested biochemical reorganization of POM during lateral transport, consistent  
473 with selective degradation and compositional restructuring rather than just uniform bulk loss. In  
474 support, PCA also showed a progressive leftward shift from MDS to Adj-W along PC1 (Fig. 5)  
475 demonstrating lateral export of POM from macroalgal beds to surrounding waters as a gradient,  
476 consistent with progressive dilution and selective transformation during fjord-scale transport of  
477 POM.

### 478 **4.3 Molecular-level evidence for macroalgal imprint and early transformation of POM**

479 Molecular fingerprints based on monosaccharides and amino acids offer direct insight into the  
480 origin, bioavailability, and early diagenetic transformation of organic matter (Grosse et al., 2021;  
481 Jo et al., 2022). Glucose is a common constituent of the macroalgal storage polysaccharide  
482 laminarin, while fucose, galactose, and uronic acids (glucuronic, mannuronic, and guluronic acids)  
483 are key monomers of structural polysaccharides such as alginates and fucans (Singh et al., 2024a).  
484 This carbohydrate pool of macroalgae is bound within structurally complex cell-wall polymers  
485 that are relatively resistant to microbial degradation (Kennedy and Blain, 2025). In contrast,  
486 phytoplankton cell walls and extracellular matrices are dominated by cellulose, and species-  
487 specific storage glucans, which are recycled relatively rapidly in surface waters (Biersmith and  
488 Benner, 1998). Glucose and galactose were observed to be the dominant monosaccharides  
489 throughout the samples, reflecting a shared baseline of organic matter likely derived from a  
490 mixture of macroalgal detritus, phytoplankton, and bacterial biomass (Li et al., 2025; Smale et al.,  
491 2022). However, the positive correlation of glucose with POC and PCHO indicated a relative  
492 enrichment of a labile, carbohydrate-rich organic matter pool at MDS where POC and PCHO were  
493 higher than Adj-W. On the other hand, the negative correlation between glucose and other  
494 monosaccharides such as galactose, mannose, mannuronic acid, ribose, and glucosamine reflected  
495 a relative increase in structurally complex, algal, microbial, and zooplankton-associated sugars  
496 during lateral transport and early diagenesis.

497 Amino acid distributions provide complementary evidence for POM source and lability  
498 patterns, as their composition reflects both the origin and degree of degradation (Grosse et al.,  
499 2021; Jo et al., 2022). The total amino acid concentrations observed in this study (24–180  $\mu\text{g L}^{-1}$ )  
500 fall within the reported values from coastal Kongsfjorden (Zhu et al., 2016) and across Fram-Strait

501 (Grosse et al., 2021). The average total amino acids were higher at MDS ( $94.8 \mu\text{g L}^{-1}$ ) than at Adj-  
502 W ( $68.4 \mu\text{g L}^{-1}$ ), with BD exhibiting the highest average concentration ( $113.0 \mu\text{g L}^{-1}$ ), indicating  
503 fresher, nitrogen-rich, proteinaceous POM in surface waters, along with elevated PPRT and low  
504 C:N ratios observed near macroalgal beds. At BD and KN, total amino acids drop by ~60–50%  
505 from MDS to Adj-W, indicating preferential microbial utilization of proteinaceous, N-rich material  
506 during lateral transport, consistent with the observed offshore increase in POC/PN and PLIP  
507 enrichment. NA and HN show mid-station or distal increases (NA\_500, HN\_1500), likely  
508 reflecting local resuspension or secondary production, supporting spatial heterogeneity as  
509 discussed before. The combined Asp + Glu content, reflecting the freshness of organic matter and  
510 the diagnostic Asp/Gly ratio, indicates the degradation state of organic matter (Machado et al.,  
511 2020; Yao et al., 2023). The decline in Glu, Asp, and Asp/Gly ratio, and the relative enrichment  
512 of Gly and Arg from MDS to Adj-W for most of the stations further provide molecular signatures  
513 for early-stage protein degradation and microbial reworking of macroalgal-derived POM during  
514 lateral transport.

515 Together, the coupled behavior of carbohydrates and amino acids demonstrated that  
516 macroalgal beds imprint surface POM with a distinct molecular signature that is progressively  
517 modified during fjord-scale export. These molecular patterns corroborate the bulk biochemical and  
518 isotopic evidences, indicating that macroalgal-derived organic matter is redistributed across  
519 coastal gradients while undergoing selective early transformation. The pronounced total  
520 monosaccharides and amino acid enrichment at BD (especially BD\_MDS), which also exhibited  
521 the highest POC and PPRT concentrations, identifies this site as a biogeochemical hotspot of  
522 macroalgal influence, reinforcing the spatial coherence of macroalgal signatures across  
523 independent biochemical proxies.

#### 524 **4.4 Brandal (BD) as a biogeochemical hotspot of macroalgal influence in Kongsfjorden**

525 BD station, among all studied stations, consistently emerged as an organic-rich site, showing  
526 characteristics of macroalgal-influenced surface POM, highlighting its role as a biogeochemical  
527 hotspot within Kongsfjorden. With the highest concentrations of POC, PN, PCHO, PPRT, total  
528 monosaccharides, and total amino acids, the BD station contributed the most in the PCA biplot  
529 (Fig. 5), which demonstrated local production and accumulation of biochemically labile organic  
530 matter within this macroalgal-dominated habitat. The strong gradient observed across PN,  $\delta^{15}\text{N}$ ,  
531 C:N, PPRT, and amino acid composition from MDS to Adj-W at BD indicated nitrogen  
532 assimilation, dominance of fresh marine organic matter in macroalgal bed, and their progressive  
533 downstream alteration. At the molecular level also, BD\_MDS was strongly enriched in glucose  
534 and other macroalgal sugars (fucose, galactose, mannuronic acid), with total monosaccharides and  
535 glucose declining offshore. Similarly, the offshore decrease in labile amino acids (e.g., Asp, Glu)  
536 provides a molecular signature for early degradation during export, indicating that the BD  
537 macroalgal bed is a major source of biochemically active POM and a key contributor to fjord-scale  
538 redistribution (van der Mheen et al., 2024).

539 Situated on the westernmost part of the south shore, BD is influenced by Atlantic water  
540 inflow, which creates relatively warmer and more saline conditions (Williams, 2017; Wilson,  
541 2022; Woelfel et al., 2014), that support abundant micro-phytobenthic and benthic mosses  
542 (Woelfel et al., 2014). At BD, macroalgal cover is not higher than other sites, yet detritus  
543 accumulation is substantial, supporting elevated benthic faunal diversity. The presence of a deep  
544 trench, combined with storm-driven transport, concentrates detritus at BD (Schimani Katherina,  
545 2019). Habitat heterogeneity further drives microbial community assembly and functional  
546 differentiation (Huang et al., 2026), reflected in high macroalgal detrital cover and meiofaunal

547 density (Schimani et al., 2022). Additionally, BD exhibits significantly lower turbidity than  
548 glacier-proximal sites, which prevents mineral masking of organic signatures and provides a stable  
549 light regime for primary producers (Bianchi et al., 2020). Collectively, these features make BD a  
550 retention zone for macroalgal detritus, acting as a biogeochemical hotspot and a critical repository  
551 for macroalgal-derived carbon. While Brandal represents a biogeochemical hotspot, its broader  
552 representativeness is constrained due to spatial variability in macroalgal structure and function  
553 across high Arctic fjords, driven by variation in latitude, ice scour, light availability, terrestrial  
554 runoff, and glacier-induced salinity and turbidity gradients (Bartsch et al., 2016). Thus, although  
555 Brandal provides a high-resolution case study, caution is required when extrapolating its  
556 biogeochemical fluxes to fjords characterized by intense glacial runoff, seasonal sea-ice cover, and  
557 a different community composition.

558

#### 559 **4.5 Implications of macroalgal-beds for Arctic coastal carbon cycling**

560 Unlike previous studies on POM in Kongsfjorden that primarily used bulk isotopes (e.g.,  $\delta^{13}\text{C}$ ,  
561  $\delta^{15}\text{N}$ ) and their ratios for source apportionment (Kuliński et al., 2014; Singh et al., 2024b), our  
562 study advances biochemical perspective by integrating molecular level biomarkers (amino acids,  
563 sugars) with spatially resolution transect. This approach shift the focus from POM origin to its  
564 functional quality, enable differentiation between labile and refractory pools. Our study  
565 demonstrates that macroalgal-dominated sites in Kongsfjorden act as hotspots of labile and  
566 bioavailable organic matter, significantly shaping the composition and lability of POM in adjacent  
567 waters. The intermediate and variable patterns observed at the few stations highlight that the  
568 influence of MDS was not uniform but forms a gradient shaped by local hydrodynamics,  
569 freshwater inputs, and nutrient availability. The strong spatial heterogeneity observed, particularly

570 the emergence of Brandal as a biogeochemical hotspot, emphasizes that macroalgal impacts on  
571 coastal carbon cycling are unevenly distributed within fjord systems. Such localized but persistent  
572 sources of organic carbon from macroalgal-beds to surrounding waters and thereby dampening  
573 seasonal variability in carbon availability (Norkko et al., 2007), enhancing benthic-pelagic food-  
574 web stability and increase ecosystem resilience to interannual fluctuations in pelagic primary  
575 production (Norkko et al., 2007; Renaud et al., 2015).

576         Although our study focused on surface waters, future research should include vertical  
577 fluxes of POM near macroalgal beds and their coupling to hydrodynamics. Additionally, effects  
578 of seasonal variability driven by glacial melt, riverine runoff, and episodic nutrient inputs at coast  
579 are important as they can alter carbon concentrations and biochemical composition, particularly in  
580 nearshore macroalgal habitats (Ager et al., 2023). Experimental studies at model sites like BD  
581 could further help in elucidating the rates of labile carbon turnover, microbial utilization, and  
582 nutrient remineralization at these sites. As macroalgal habitats are expanding under ongoing  
583 warming, resolving the contribution of macroalgal biomass and beds-associated organic matter  
584 dynamics in coastal biogeochemistry would be important for estimating Arctic carbon budgets and  
585 ecosystem functioning.

586

## 587 **Conclusion**

588 The present study provides new insights into the role of Arctic macroalgal beds as active drivers  
589 of coastal particulate organic matter dynamics in Kongsfjorden, an Arctic fjord. By integrating  
590 bulk biogeochemical properties, stable isotopes, bio-polymeric composition, and molecular  
591 biomarkers, we demonstrate that macroalgal habitats imprint surface waters with a distinct  
592 biochemical and molecular signature. Elevated concentrations of POC, PN, carbohydrates,

593 proteins, monosaccharides, and amino acids at macroalgal-dominated sites indicate that  
594 macroalgal beds act as localized sources of biochemically labile organic matter to the overlying  
595 water column. Systematic offshore declines in bulk parameters, together with internal  
596 reorganization of bio-polymeric and molecular composition, reveal that macroalgal-beds derived  
597 POM is efficiently exported across fjord-scale gradients and undergoes selective early-stage  
598 transformation during lateral transport. The muted bulk isotopic gradients further indicate that  
599 macroalgal influence is expressed through continuous mixing and biochemical restructuring of a  
600 heterogeneous particulate pool rather than simple replacement of pelagic organic matter. A  
601 pronounced spatial gradient was observed across the stations, within which Brandal emerged as a  
602 distinct biogeochemical hotspot of macroalgal-associated organic matter dynamics, as supported  
603 by our multiproxy study. Overall, our findings show that macroalgal beds function as dynamic  
604 benthic–pelagic coupling zones that redistribute and transform organic carbon beyond their  
605 immediate habitat. As macroalgal cover continues to expand along Arctic coastlines under climate  
606 warming, their contribution to coastal carbon fluxes is likely to intensify, with important  
607 implications for Arctic carbon budgets and ecosystem functioning.

608

609 **Data availability.** The data are available in the Zenodo repository at:  
610 <https://doi.org/10.5281/zenodo.18457176> (Jagtap et al., 2026).

611

612 **Author contributions.** ASJ and AS conceptualized the study with input from AJ. AS and AJ  
613 conducted the fieldwork, while laboratory analyses were performed by ASJ and NR. MT analyzed  
614 the elemental and isotopic data. All authors were involved in the interpretation of the results, the  
615 revision, and the writing of the final version of the paper.

616

617 **Competing interests.** The corresponding author has declared that none of the authors has any  
618 competing interests.

619

620 **Acknowledgement.** We extend our gratitude to the Director of the National Centre for Polar and  
621 Ocean Research for their support in this work. We acknowledge funding from the Ministry of  
622 Earth Sciences. We are thankful to Dr. Biswajit Roy, Dr. PV Bhaskar, and Ms. Viola Rodrigues  
623 for sampling assistance, nutrient and EA-IRMS analysis, respectively.

624

625 **Financial Support.** This research was funded by the National Centre for Polar and Ocean  
626 Research (NCPOR), Ministry of Earth Sciences (MoES), India.

627

## 628 **References**

629 Ager, T. G., Krause-Jensen, D., Olesen, B., Carlson, D. F., Winding, M. H. S., and Sejr, M. K.:  
630 Macroalgal habitats support a sustained flux of floating biomass but limited carbon export  
631 beyond a Greenland fjord, *Sci. Total Environ.*, 872, 162224,  
632 <https://doi.org/10.1016/j.scitotenv.2023.162224>, 2023.

633 Assis, J., Serrão, E. A., Duarte, C. M., Fragkopoulou, E., and Krause-Jensen, D.: Major  
634 Expansion of Marine Forests in a Warmer Arctic, *Front. Mar. Sci.*, 9, 1–10,  
635 <https://doi.org/10.3389/fmars.2022.850368>, 2022.

636 Bartsch, I., Paar, M., Fredriksen, S., Schwanitz, M., Daniel, C., Hop, H., and Wiencke, C.:  
637 Changes in kelp forest biomass and depth distribution in Kongsfjorden, Svalbard, between 1996–  
638 1998 and 2012–2014 reflect Arctic warming, *Polar Biol.*, 39, 2021–2036,  
639 <https://doi.org/10.1007/s00300-015-1870-1>, 2016.

640 Bianchi, T. S., Arndt, S., Austin, W. E. N., Benn, D. I., Bertrand, S., Cui, X., Faust, J. C.,  
641 Koziarowska-makuch, K., Moy, C. M., Savage, C., Smeaton, C., Smith, R. W., and Syvitski, J.:  
642 Earth-Science Reviews Fjords as Aquatic Critical Zones ( ACZs ), *Earth-Science Rev.*, 203,  
643 103145, <https://doi.org/10.1016/j.earscirev.2020.103145>, 2020.

- 644 Biersmith, A. and Benner, R.: Carbohydrates in phytoplankton and freshly produced dissolved  
645 organic matter, *Mar. Chem.*, 63, 131–144, [https://doi.org/10.1016/S0304-4203\(98\)00057-7](https://doi.org/10.1016/S0304-4203(98)00057-7),  
646 1998.
- 647 Buchholz, C. M. and Wiencke, C.: Working on a baseline for the Kongsfjorden food web:  
648 production and properties of macroalgal particulate organic matter (POM), *Polar Biol.*, 39, 2053–  
649 2064, <https://doi.org/10.1007/s00300-015-1828-3>, 2016.
- 650 Burfeid-Castellanos, A. M., Martín-Martín, R. P., Kloster, M., Angulo-Preckler, C., Avila, C.,  
651 and Beszteri, B.: Epiphytic diatom community structure and richness is determined by  
652 macroalgal host and location in the South Shetland Islands (Antarctica), *PLoS One*, 16, 1–21,  
653 <https://doi.org/10.1371/journal.pone.0250629>, 2021.
- 654 Carlson, D. F., Suzuki, N., Carrasco, R., Filbee-Dexter, K., Gillard, L. C., Myers, P. G., Queirós,  
655 A. M., Assis, J., Duarte, C. M., Sejr, M., and Krause-Jensen, D.: Ocean transport and vertical  
656 mixing connect Greenland’s macroalgae to deep ocean carbon sinks, *Sci. Total Environ.*, 1012,  
657 <https://doi.org/10.1016/j.scitotenv.2025.181247>, 2026.
- 658 Castro de la Guardia, L., Bartsch, I., Hop, H., Niedzwiedz, S., Düsedau, L., Diehl, N., Krause-  
659 Jensen, D., Sejr, M., Ager, T. G., Gattuso, J. P., Schlegel, R. W., Miller, C. A., Filbee-Dexter, K.,  
660 and Duarte, P.: Predicting potential Arctic kelp distribution and lower-depth biomass from  
661 seafloor irradiance, *Limnol. Oceanogr. Methods*, <https://doi.org/10.1002/lom3.70018>, 2025.
- 662 Chen, S., Xu, K., Ji, D., Wang, W., Xu, Y., Chen, C., and Xie, C.: Release of dissolved and  
663 particulate organic matter by marine macroalgae and its biogeochemical implications, *Algal*  
664 *Res.*, 52, 102096, <https://doi.org/10.1016/j.algal.2020.102096>, 2020.
- 665 Dai, A., Luo, D., Song, M., and Liu, J.: Arctic amplification is caused by sea-ice loss under  
666 increasing CO<sub>2</sub>, *Nat. Commun.*, 10, 1–13, <https://doi.org/10.1038/s41467-018-07954-9>, 2019.
- 667 Danovaro, R., Dell’Anno, A., and Fabiano, M.: Bioavailability of organic matter in the  
668 sediments of the Porcupine Abyssal Plain, northeastern Atlantic, *Mar. Ecol. Prog. Ser.*, 220, 25–  
669 32, <https://doi.org/10.3354/meps220025>, 2001.
- 670 Duarte, C. M., Losada, I. J., Hendriks, I. E., Mazarrasa, I., and Marbà, N.: The role of coastal  
671 plant communities for climate change mitigation and adaptation, *Nat. Clim. Chang.*, 3, 961–968,  
672 <https://doi.org/10.1038/nclimate1970>, 2013.
- 673 Dubois, M., Gilles, K. A., Hamilton, J. K., Rebers, P. A., and Smith, F.: Colorimetric Method for  
674 Determination of Sugars and Related Substances, 350–356, 1956.
- 675 Düsedau, L., Fredriksen, S., Brand, M., Fischer, P., Karsten, U., Bischof, K., Savoie, A., and  
676 Bartsch, I.: Kelp forest community structure and demography in Kongsfjorden (Svalbard) across  
677 25 years of Arctic warming, *Ecol. Evol.*, 14, 1–25, <https://doi.org/10.1002/ece3.11606>, 2024.
- 678 Dyer, D. C., Butler, M. J., Smit, A. J., Anderson, R. J., and Bolton, J. J.: Kelp forest POM during

679 upwelling and downwelling conditions: Using stable isotopes to differentiate between detritus  
680 and phytoplankton, *Mar. Ecol. Prog. Ser.*, 619, 17–34, <https://doi.org/10.3354/meps12941>, 2019.

681 Elliott Smith, E. A. and Fox, M. D.: Characterizing energy flow in kelp forest food webs: a  
682 geochemical review and call for additional research, *Ecography (Cop.)*, 2022, 1–16,  
683 <https://doi.org/10.1111/ecog.05566>, 2022.

684 Fabiano, M., Povero, P., and Danovaro, R.: Distribution and composition of particulate organic  
685 matter in the Ross Sea (Antarctica), *Polar Biol.*, 13, 525–533,  
686 <https://doi.org/10.1007/BF00236394>, 1993.

687 Filbee-Dexter, K. and Wernberg, T.: Substantial blue carbon in overlooked Australian kelp  
688 forests, *Sci. Rep.*, 10, 1–6, <https://doi.org/10.1038/s41598-020-69258-7>, 2020.

689 Filbee-Dexter, K., MacGregor, K. A., Lavoie, C., Garrido, I., Goldsmit, J., Castro de la Guardia,  
690 L., Howland, K. L., Johnson, L. E., Konar, B., McKindsey, C. W., Mundy, C. J., Schlegel, R.  
691 W., and Archambault, P.: Sea Ice and Substratum Shape Extensive Kelp Forests in the Canadian  
692 Arctic, *Front. Mar. Sci.*, 9, 1–27, <https://doi.org/10.3389/fmars.2022.754074>, 2022.

693 FOLCH, J., LEES, M., and SLOANE STANLEY, G. H.: A simple method for the isolation and  
694 purification of total lipides from animal tissues., *J. Biol. Chem.*, 226, 497–509,  
695 [https://doi.org/10.1016/s0021-9258\(18\)64849-5](https://doi.org/10.1016/s0021-9258(18)64849-5), 1957.

696 Fredriksen, S.: Food web studies in a Norwegian kelp forest based on stable isotope ( $\delta^{13}\text{C}$  and  
697  $\delta^{15}\text{N}$ ) analysis, *Mar. Ecol. Prog. Ser.*, 260, 71–81, <https://doi.org/10.3354/meps260071>, 2003.

698 Gao, J., Wang, Y., Pan, S., Zhang, R., Li, J., and Bai, F.: Spatial distributions of organic carbon  
699 and nitrogen and their isotopic compositions in sediments of the Changjiang Estuary and its  
700 adjacent sea area, *J. Geogr. Sci.*, 18, 46–58, <https://doi.org/10.1007/s11442-008-0046-0>, 2008.

701 Grasshoff: *Methods\_Seawater\_Analysis*, 2009.

702 Grosse, J., Nöthig, E. M., Torres-Valdés, S., and Engel, A.: Summertime Amino Acid and  
703 Carbohydrate Patterns in Particulate and Dissolved Organic Carbon Across Fram Strait, *Front.*  
704 *Mar. Sci.*, 8, <https://doi.org/10.3389/fmars.2021.684675>, 2021.

705 Huang, J., Cai, M., Han, M., Fang, B., Dong, L., Zhang, G., Han, J., Li, S., Rustamova, N., Liu,  
706 Y., Li, W., Jiang, H., Huang, J., Cai, M., Han, M., Fang, B., Dong, L., Zhang, G., Han, J., Li, S.,  
707 Rustamova, N., Liu, Y., Li, W., and Jiang, H.: Habitat heterogeneity drives microbial community  
708 assembly and functional specialization in extreme arid ecosystems and functional specialization  
709 in extremely arid ecosystems, 92, <https://doi.org/10.1128/aem.02588-25>, 2026.

710 Jagtap, A., Singh, A., jain, . anand ., Tiwari, M., & Raj, N.: Particulate Organic Matter  
711 composition in and around macroalgal beds in Kongsfjorden, Arctic, *Zenodo*,  
712 <https://doi.org/https://doi.org/10.5281/zenodo.18457176>, 2026.

- 713 Jain, A., Krishnan, K. P., Singh, A., Thomas, F. A., Begum, N., Tiwari, M., Bhaskar, V. P., and  
714 Gopinath, A.: Biochemical composition of particles shape particle-attached bacterial community  
715 structure in a high Arctic fjord, *Ecol. Indic.*, 102, 581–592,  
716 <https://doi.org/10.1016/j.ecolind.2019.03.015>, 2019.
- 717 Jiang, H., Lv, Q., Yang, J., Wang, B., Dong, H., Gonsior, M., and Schmitt-kopplin, P.: Organic  
718 Geochemistry Molecular composition of dissolved organic matter in saline lakes of the Qing-  
719 Tibetan Plateau, *Org. Geochem.*, 167, 104400,  
720 <https://doi.org/10.1016/j.orggeochem.2022.104400>, 2022.
- 721 Jo, N., La, H. S., Kim, J. H., Kim, K., Kim, B. K., Kim, M. J., Son, W., and Lee, S. H.: Different  
722 Biochemical Compositions of Particulate Organic Matter Driven by Major Phytoplankton  
723 Communities in the Northwestern Ross Sea, *Front. Microbiol.*, 12,  
724 <https://doi.org/10.3389/fmicb.2021.623600>, 2021.
- 725 Jo, N., Youn, S. H., Joo, H. T., Jang, H. K., Kim, Y., Park, S., Kim, J., Kim, K., Kang, J. J., and  
726 Lee, S. H.: Seasonal variations in biochemical (biomolecular and amino acid) compositions and  
727 protein quality of particulate organic matter in the Southwestern East/Japan Sea, *Front. Mar. Sci.*,  
728 9, <https://doi.org/10.3389/fmars.2022.979137>, 2022.
- 729 Karl Attard; Rakesh Kumar Singh, J.-P., Gattusof, Karen Filbee-Dexter, Dorte Krause-Jensen,  
730 M. K., and Mikael K. Sejr, Philippe Archambault, Marcel Babin, Simon Bélanger, Peter Berg,  
731 Ronnie N. Glud, Kasper Hancke, Stefan Jänicke, Jing Qin, Søren Rysgaard, Esben B. Sørensen,  
732 Foucaut Tachon, Frank Wenzhöfer, and M. A.: Seafloor primary production in a changing  
733 Arctic Ocean, *PNAS*, 121, e2303366121, 2024.
- 734 Kennedy, J. R. and Blain, C. O.: A systematic review of marine macroalgal degradation: Toward  
735 a better understanding of macroalgal carbon sequestration potential, *J. Phycol.*, 61, 399–432,  
736 <https://doi.org/10.1111/jpy.70031>, 2025.
- 737 Kim, J., Jo, N., Park, J., Kim, K., Park, S., Kim, Y., Kim, J., Kim, B. K., Lee, B., and Lee, S. H.:  
738 Different amino acid compositions and food quality of particulate organic matter driven by two  
739 major phytoplankton groups in the Ross Sea, *J. Sea Res.*, 201, 102524,  
740 <https://doi.org/10.1016/j.seares.2024.102524>, 2024.
- 741 Krause-Jensen, D. and Duarte, C. M.: Substantial role of macroalgae in marine carbon  
742 sequestration, *Nat. Geosci.*, 9, 737–742, <https://doi.org/10.1038/ngeo2790>, 2016.
- 743 Krause-Jensen, D., Archambault, P., Assis, J., Bartsch, I., Bischof, K., Filbee-Dexter, K.,  
744 Dunton, K. H., Maximova, O., Ragnarsdóttir, S. B., Sejr, M. K., Simakova, U., Spiridonov, V.,  
745 Wegeberg, S., Winding, M. H. S., and Duarte, C. M.: Imprint of Climate Change on Pan-Arctic  
746 Marine Vegetation, *Front. Mar. Sci.*, 7, 1–28, <https://doi.org/10.3389/fmars.2020.617324>, 2020.
- 747 Kuliński, K., Kędra, M., Legeżyńska, J., Gluchowska, M. and Zaborska, A.: Particulate organic  
748 matter sinks and sources in high Arctic fjord. *Journal of Marine Systems*, 139, 27–37,  
749 <https://doi.org/10.1016/j.jmarsys.2014.04.018>, 2014.

- 750 Kuzyk, Z. Z. A., Macdonald, R. W., Tremblay, J. É., and Stern, G. A.: Elemental and stable  
751 isotopic constraints on river influence and patterns of nitrogen cycling and biological  
752 productivity in Hudson Bay, *Cont. Shelf Res.*, 30, 163–176,  
753 <https://doi.org/10.1016/j.csr.2009.10.014>, 2010.
- 754 Li, H., Zhang, Z., Chen, J., Nair, S., Xiong, T., Zhao, H., He, D., Lee, K., Jiao, N., and Zhang,  
755 Y.: Fate and carbon sequestration potential of sunken macroalgae in coastal oceans from long-  
756 term microbial degradation perspective, *Natl. Sci. Rev.*, 12, <https://doi.org/10.1093/nsr/nwaf273>,  
757 2025.
- 758 Lobbes, J. M., Fitznar, H. P., and Kattner, G.: Biogeochemical characteristics of dissolved and  
759 particulate organic matter, *Geochim. Cosmochim. Acta*, 64, 2973–2983, 2000.
- 760 Machado, M., Machado, S., Pimentel, F. B., Freitas, V., Alves, R. C., and Oliveira, M. B. P. P.:  
761 Amino acid profile and protein quality assessment of macroalgae produced in an integrated  
762 multi-trophic aquaculture system, *Foods*, 9, <https://doi.org/10.3390/foods9101382>, 2020.
- 763 Mathew, S., Hong, J. K., Kim, J. H., Chen, M., and Hur, J.: Terrestrial inputs of nutrients and  
764 dissolved organic carbon to the Arctic Ocean and their influence on primary production, *Mar.*  
765 *Environ. Res.*, 209, 107182, <https://doi.org/10.1016/j.marenvres.2025.107182>, 2025.
- 766 McGovern, M., Pavlov, A. K., Deininger, A., Granskog, M. A., Leu, E., Søreide, J. E., and Poste,  
767 A. E.: Terrestrial Inputs Drive Seasonality in Organic Matter and Nutrient Biogeochemistry in a  
768 High Arctic Fjord System (Isfjorden, Svalbard), *Front. Mar. Sci.*, 7, 1–15,  
769 <https://doi.org/10.3389/fmars.2020.542563>, 2020.
- 770 van der Mheen, M., Wernberg, T., Pattiaratchi, C., Pessarrodona, A., Janekovic, I., Simpkins, T.,  
771 Hovey, R., and Filbee-Dexter, K.: Substantial kelp detritus exported beyond the continental shelf  
772 by dense shelf water transport, *Sci. Rep.*, 14, 1–12, <https://doi.org/10.1038/s41598-023-51003-5>,  
773 2024.
- 774 Niedzwiedz, S., Voigt, C., Andersen, S., Diehl, N., Descôteaux, R., Damsgård, B., and Bischof,  
775 K.: Biochemistry of Arctic kelp specimens is conditioned by the local environment, *Mar.*  
776 *Environ. Res.*, 212, <https://doi.org/10.1016/j.marenvres.2025.107604>, 2025.
- 777 Norkko, A., Thrush, S. F., Cummings, V. J., Gibbs, M. M., Andrew, N. L., Norkko, J., and  
778 Schwarz, A. M.: Trophic structure of coastal Antarctic food webs associated with changes in sea  
779 ice and food supply, *Ecology*, 88, 2810–2820, <https://doi.org/10.1890/06-1396.1>, 2007.
- 780 Ørberg, S. B., Duarte, C. M., Geraldi, N. R., Sejr, M. K., Wegeberg, S., Hansen, J. L. S., and  
781 Krause-Jensen, D.: Prevalent fingerprint of marine macroalgae in arctic surface sediments, *Sci.*  
782 *Total Environ.*, 898, <https://doi.org/10.1016/j.scitotenv.2023.165507>, 2023.
- 783 Ortega, A., Geraldi, N. R., Alam, I., Kamau, A. A., Acinas, S. G., Logares, R., Gasol, J. M.,  
784 Massana, R., Krause-Jensen, D., and Duarte, C. M.: Important contribution of macroalgae to  
785 oceanic carbon sequestration, *Nat. Geosci.*, 12, 748–754, <https://doi.org/10.1038/s41561-019->

786 0421-8, 2019.

787 Pedersen, M. F., Filbee-Dexter, K., Frisk, N. L., Sárossy, Z., and Wernberg, T.: Carbon  
788 sequestration potential increased by incomplete anaerobic decomposition of kelp detritus, *Mar.*  
789 *Ecol. Prog. Ser.*, 660, 53–67, <https://doi.org/10.3354/meps13613>, 2021.

790 Pessarrodona, A., Assis, J., Filbee-Dexter, K., Burrows, M. T., Gattuso, J. P., Duarte, C. M.,  
791 Krause-Jensen, D., Moore, P. J., Smale, D. A., and Wernberg, T.: Global seaweed productivity,  
792 *Sci. Adv.*, 8, <https://doi.org/10.1126/sciadv.abn2465>, 2022.

793 Pineault, S., Tremblay, J. É., Gosselin, M., Thomas, H., and Shadwick, E.: The isotopic signature  
794 of particulate organic C and N in bottom ice: Key influencing factors and applications for tracing  
795 the fate of ice-algae in the Arctic Ocean, *J. Geophys. Res. Ocean.*, 118, 287–300,  
796 <https://doi.org/10.1029/2012JC008331>, 2013.

797 Rantanen, M., Karpechko, A. Y., Lipponen, A., Nordling, K., Hyvärinen, O., Ruosteenoja, K.,  
798 Vihma, T., and Laaksonen, A.: The Arctic has warmed nearly four times faster than the globe  
799 since 1979, *Commun. Earth Environ.*, 3, 1–10, <https://doi.org/10.1038/s43247-022-00498-3>,  
800 2022.

801 Renaud, P. E., Løkken, T. S., Jørgensen, L. L., Berge, J., and Johnson, B. J.: Macroalgal detritus  
802 and food-web subsidies along an Arctic fjord depth-gradient, *Front. Mar. Sci.*, 2, 1–15,  
803 <https://doi.org/10.3389/fmars.2015.00031>, 2015.

804 Roy, B., Singh, A. and Tiwari, M.: Tracing macroalgal-induced changes in carbon dynamics of  
805 high-Arctic fjords using biomarker fingerprinting. *J. Geophys. Res. Ocean.*, 130(4),  
806 p.e2024JC021900, <https://doi.org/10.1029/2024JC021900>, 2025.

807 Schimani, K., Zacher, K., Jerosch, K., Pehlke, H., Wiencke, C., and Bartsch, I.: Video survey of  
808 deep benthic macroalgae and macroalgal detritus along a glacial Arctic fjord: Kongsfjorden  
809 (Spitsbergen), *Polar Biol.*, 45, 1291–1305, <https://doi.org/10.1007/s00300-022-03072-x>, 2022.

810 Schimani Katherina: Macroalgal communities in Kongsfjorden, Spitsbergen-Analysis of video  
811 transects (Doctoral dissertation), 2019.

812 Singh, A., Pal, B., and Singh, K. S.: Carbohydrate and pigment composition of macroalgae in a  
813 kelp-dominated Arctic fjord, *Reg. Stud. Mar. Sci.*, 77, 103644,  
814 <https://doi.org/10.1016/j.rsma.2024.103644>, 2024a.

815 Singh, A., Jain, A., Singh, R., Singh, K. S., Roy, B., Tiwari, M., David T., D., and Jagtap, A.:  
816 Tracing marine and terrestrial biochemical signatures of particulate organic matter in an Arctic  
817 fjord (Kongsfjorden), *Mar. Chem.*, 267, 104468,  
818 <https://doi.org/10.1016/j.marchem.2024.104468>, 2024b.

819 Smale, D. A., Pessarrodona, A., King, N., and Moore, P. J.: Examining the production, export,  
820 and immediate fate of kelp detritus on open-coast subtidal reefs in the Northeast Atlantic,

- 821 *Limnol. Oceanogr.*, 67, S36–S49, <https://doi.org/10.1002/lno.11970>, 2022.
- 822 Stanca, E. and Parsons, M. L.: Examining the dynamic nature of epiphytic microalgae in the  
823 Florida Keys: What factors influence community composition?, *J. Exp. Mar. Bio. Ecol.*, 538,  
824 <https://doi.org/10.1016/j.jembe.2021.151538>, 2021.
- 825 Taylor Simpkins, Mirjam Van Der Mheen, Morten F. Pedersen, A. P. and Chari Pattiaratchi,  
826 Thomas Wernberg, K. F.-D.: Macroalgae detritus decomposition and cross-shelf carbon export  
827 from shallow and deep reefs, <https://doi.org/10.1002/lno.70006>, 2025.
- 828 Tselepides, A., Polychronaki, T., Marrale, D., Akoumianaki, I., Dell’Anno, A., Pusceddu, A.,  
829 and Danovaro, R.: Organic matter composition of the continental shelf and bathyal sediments of  
830 the Cretan Sea (NE Mediterranean), *Prog. Oceanogr.*, 46, 311–344,  
831 [https://doi.org/10.1016/S0079-6611\(00\)00024-0](https://doi.org/10.1016/S0079-6611(00)00024-0), 2000.
- 832 Upreti, G. C., Ratcliff, R. A., and Riches, P. C.: Protein Estimation in Tissues Containing High  
833 Levels of Lipid : Modifications to Lowry ’ s Method of Protein Determination Effect of  
834 Detergents upon NADPH- Generating Enzymes Protein Estimation by the BCA Method, 427,  
835 421–427, 1988.
- 836 Velázquez-Ochoa, R., Ochoa-Izaguirre, M. J., and Soto-Jiménez, M. F.: An analysis of the  
837 variability in  $\delta^{13}\text{C}$  in macroalgae from the Gulf of California: Indicative of carbon concentration  
838 mechanisms and isotope discrimination during carbon assimilation, *Biogeosciences*, 19, 1–27,  
839 <https://doi.org/10.5194/bg-19-1-2022>, 2022.
- 840 Vidal M, Aspillaga E, Teixidor-Toneu I, Delgado-Huertas A.: Lateral Transport of N-rich  
841 dissolved organic matter strengthens phosphorus deficiency in western subtropical North  
842 Atlantic. *Global Biogeochem. Cyc.*, 32, 1350-66, <https://doi.org/10.1029/2017GB005868>, 2018.
- 843 Watanabe, K., Yoshida, G., Hori, M., Umezawa, Y., Moki, H., and Kuwae, T.: Macroalgal  
844 metabolism and lateral carbon flows create extended atmospheric  $\text{CO}_2$  sinks, *Biogeosciences*  
845 *Discuss.*, 1–25, <https://doi.org/10.5194/bg-17-2425-2020>, 2019.
- 846 Williams, L., Borchhardt, N., Colesie, C., Baum, C., Komsic-Buchmann, K., Rippin, M., Becker,  
847 B., Karsten, U., Büdel, B.: Biological soil crusts of arctic Svalbard and of Livingston Island,  
848 Antarctica. *Polar Biol.*, 40, 399-411, <https://doi.org/10.1007/s00300-016-1967-1>, 2017.
- 849 Wilson, S.K., Fulton, C.J., Graham, N.A., A Abesamis, R., Berkström, C., Coker, D.J.,  
850 Depczynski, M., Evans, R.D., Fisher, R., Goetze, J. and Hoey, A.: The contribution of  
851 macroalgae-associated fishes to small-scale tropical reef fisheries. *Fish Fish.*, 23, 847-861,  
852 <https://doi.org/10.1111/faf.12653>, 2022.
- 853 Woelfel, J., Eggert, A., and Karsten, U.: Marginal impacts of rising temperature on Arctic  
854 benthic microalgae production based on in situ measurements and modelled estimates, *Mar.*  
855 *Ecol. Prog. Ser.*, 501, 25–40, <https://doi.org/10.3354/meps10688>, 2014.

- 856 Yang, J., Jiang, H., Liu, W., Huang, L., Huang, J., and Wang, B.: Potential utilization of  
857 terrestrially derived dissolved organic matter by aquatic microbial communities in saline lakes,  
858 *ISME J.*, 2313–2324, <https://doi.org/10.1038/s41396-020-0689-0>, 2020.
- 859 Yao, X., Fan, T., Gao, G., Liu, L., Chao, J., and Liu, H.: Spatiotemporal pattern and  
860 biodegradation process of amino acids in the large shallow eutrophic lake Taihu, China, *Environ.*  
861 *Sci. Pollut. Res.*, 30, 12584–12595, <https://doi.org/10.1007/s11356-022-23014-8>, 2023.
- 862 Zhu, Z. Y., Wu, Y., Liu, S. M., Wenger, F., Hu, J., Zhang, J., and Zhang, R. F.: Organic carbon  
863 flux and particulate organic matter composition in Arctic valley glaciers: Examples from the  
864 Bayelva River and adjacent Kongsfjorden, *Biogeosciences*, 13, 975–987,  
865 <https://doi.org/10.5194/bg-13-975-2016>, 2016.
- 866